Turbulence Closure Models for Computational Fluid Dynamics

Paul A. Durbin
Iowa State University, Ames, IA, USA

1 INTRODUCTION: THE ROLE OF STATISTICAL CLOSURE

Turbulence is the highly irregular flow of fluids. It is governed by the exact, Navier–Stokes, momentum equations; but it is of little comfort to realize that turbulence is just a particular type of solution to these laws of fluid dynamics. Although its full disorderliness can be directly simulated on the computer (see **Turbulence Direct Numerical Simulation and Large-Eddy Simulation**), that is too expensive computationally and too fine a level of detail for many practical purposes. When the need is for timely prediction of the flow fields in practical devices, statistical moment closures of the type discussed in this chapter are invariably invoked.

There are good reasons why most of the analytical approaches to turbulence prediction resort to statistical descriptions. The average over an ensemble of realizations of turbulent flow produces a reproducible, smooth flow field. Quantities such as the mean and variance of the velocity provide definite values to be used in engineering analysis. It would seem that the smoother, averaged flow also is more amenable to computation than the instantaneous, random flow. Unfortunately, there are no exact equations governing this smooth, average field. This is where closure modeling, the subject of this chapter, comes into play.

For historical reasons, the mean velocity is called the *Reynolds-averaged velocity* and the equations obtained by averaging the Navier–Stokes equations are called the RANS (Reynolds-averaged Navier–Stokes) equations. Figure 1 contrasts an instantaneous, random velocity field, to its ensemble average. The former is a direct numerical simulation; the latter is its Reynolds average. Statistical closure models are meant to predict the field shown in (b), without having to average over an ensemble of fields shown in (a). To accomplish this, new equations must be added to Navier–Stokes so that the average effects of turbulent mixing are represented. These extra, turbulence closure equations, by necessity, contain empirical coefficients; this is not a shortcoming, it is usually the only prospect one has to obtain predictions of engineering accuracy with manageable computing times.

2 REYNOLDS-AVERAGED NAVIER–STOKES EQUATIONS

The equations that underlie single point moment closure models will be briefly summarized. Lengthy discussions of their derivation and interpretation can be found in texts on turbulence (Pope, 2000; Durbin and Reif, 2010).

Encyclopedia of Computational Mechanics Second Edition,
Edited by Erwin Stein, René de Borst and Thomas J.R. Hughes.

DOI: 10.1002/9781119176817.ecm2061

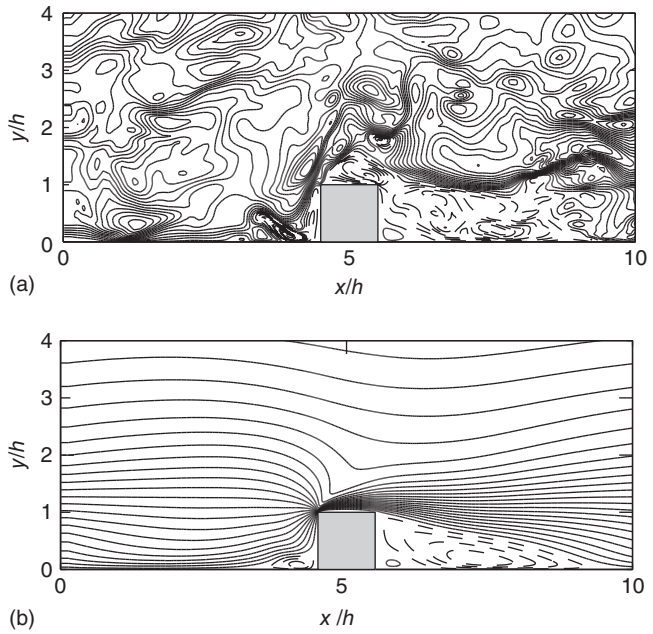

Figure 1. U contours in a ribbed channel. (a) Instantaneous u field (DNS) and (b) ensemble average (RANS). (Reproduced from Ikeda and Durbin (2002) courtesy of T. Ikeda. © Ikeda & Durbin, 2002.)

We introduce the ensemble average of a random function $f(\boldsymbol{x}, t)$

$$\bar{f}(\boldsymbol{x}, t) = \lim_{N\to\infty} \frac{1}{N} \sum_{i=1}^{N} f_i(\boldsymbol{x}, t) \quad \text{or} \quad \bar{f} = \int f' P(f') \mathrm{d}f' \tag{1}$$

for either discrete samples or a continuous probability density. If the random process is statistically stationary, the above can be replaced by a time average

$$\bar{f}(\boldsymbol{x}) = \lim_{t\to\infty} \frac{1}{t} \int_0^t f(\boldsymbol{x}; t') \mathrm{d}t' \tag{2}$$

The caveat of statistical stationarity means that the statistics are independent of the time origin; in other words, $f(t)$ and $f(t + t_0)$ have the same statistical properties for any t_0. If f is statistically homogeneous in direction y,

$$\bar{f} = \lim_{y\to\infty} \frac{1}{y} \int_0^y f(x, z, t; y') \mathrm{d}y' \tag{3}$$

can be used, the result being independent of the direction of homogeneity, y.

The Reynolds decomposition of the random variable, $\tilde{u}$, is into a sum of its mean and a fluctuation,

$$\tilde{u} = U + u \tag{4}$$

where $U \equiv \bar{\tilde{u}}$. The fluctuation u is defined to be the turbulence. For variable density, a convenient formalism consists of the introduction of the density-weighted averages, $\overline{\rho} U \equiv \overline{\rho \tilde{u}}$ and $\overline{\rho}\ \overline{u_i u_j} \equiv \overline{\rho u_i u_j}$. We will allow for density variation, but we are not primarily concerned with direct effects of compressibility on the turbulence. Ignoring compressibility in the turbulence equations, although not in the mean flow, is generally acceptable well beyond transonic speeds (Barre *et al*., 2002).

The turbulence problem, as presently formulated, is to describe the statistics of the velocity field, without access to realizations of the random flow. It seems sensible to start by attempting to derive equations for statistics. Toward this end, averages of the Navier–Stokes equations can be formed, in hopes of finding equations that govern the mean velocity, the velocity covariances ($\overline{u_i u_j}$), and so on. Regrettably, the averaged equations are unclosed – meaning that each set of statistical moment equations contains more unknowns than equations. In that sense, they fall short of any ambition to arrive at governing laws for statistics. However, the Reynolds-averaged equations give an insight into the factors that govern the evolution of the mean flow and Reynolds stresses; they also form the basis for the closure models to be discussed subsequently.

The momentum and continuity equations governing (Newtonian) viscous flow, whether turbulent or laminar, are White (1991)

$$\begin{aligned} \partial_t \rho \tilde{u}_i + \partial_j \rho \tilde{u}_j \tilde{u}_i &= -\partial_i \tilde{p} + \partial_j [\mu(\partial_i \tilde{u}_j + \partial_j \tilde{u}_i)] \\ \partial_t \rho + \partial_j \rho \tilde{u}_j &= 0 \end{aligned} \tag{5}$$

If the Reynolds decomposition (4) is substituted into (5) and the result is averaged, the RANS equations

$$\begin{aligned} \overline{\rho} \partial_t U_i + \overline{\rho} U_j \partial_j U_i &= -\partial_i P + \partial_j [\overline{\mu}(\partial_i U_j + \partial_j U_i)] - \boldsymbol{\partial_j(\overline{\rho}\ \overline{u_j u_i})} \\ \partial_t \overline{\rho} + \partial_j \overline{\rho} U_j &= 0 \end{aligned} \tag{6}$$

are obtained. The viscous term invokes an assumption that density fluctuations are not significant in viscous regions. Equations (6) for the mean velocity are equivalent to equations (5) for the total instantaneous velocity, except for the last, highlighted, term of the momentum equation. This term is a derivative of the Reynolds stress tensor. It comes from the convective derivative, so the Reynolds stresses represent the averaged effect of turbulent convection. Any understanding of the nature of closure models relies on recognizing that they represent this ensemble averaged effect, which, for instance, diffuses mean momentum.

The mean flow equations (6) are unclosed because they contain six unknown components of the Reynolds stress

tensor, $\overline{\boldsymbol{uu}}$. These derive from averaging the quadratic nonlinearity of the Navier–Stokes equations. Any nonlinearity causes moment equations to be unclosed: here, the first moment equation contains second moments; the second moment equation will contain third moments; and so on up the hierarchy. The second moment is the highest level considered in most single point moment closure modeling.

Dynamical equations for the Reynolds stress tensor can be derived from the equation for the fluctuating velocity. For simplicity, we consider constant viscosity and solenoidal velocity fluctuations, $\nabla \cdot \boldsymbol{u} = 0$, so $\rho' \ll \rho$. After subtracting (6) from (5), multiplying by u_j, averaging, and adding the result to the same equation with i and j reversed

$$\partial_t \overline{u_i u_j} + U_k \partial_k \overline{u_i u_j} = \mathcal{P}_{ij} + \wp_{ij} - \frac{2}{3}\varepsilon\delta_{ij} + T_{ij} + \frac{1}{\rho}\partial_k(\mu \partial_k \overline{u_i u_j}) \tag{7}$$

is obtained. Definitions and terminology for the various terms on the right are

$$\left.\begin{aligned}
&\mathcal{P}_{ij} \equiv -\overline{u_j u_k}\partial_k U_i - \overline{u_i u_k}\partial_k U_j && \text{production}\\
&\wp_{ij} \equiv (-\overline{u_j \partial_i p} - \overline{u_i \partial_j p} \\
&\qquad + (2/3)\delta_{ij}\overline{u_k \partial_k p})/\rho \\
&\qquad - 2\nu\overline{\partial_k u_i \partial_k u_j} + (2/3)\delta_{ij}\varepsilon && \text{redistribution}\\
&\varepsilon \equiv \nu\,\overline{\partial_k u_j \partial_k u_j} && \text{dissipation}\\
&T_{ij} \equiv -(\partial_k \rho\,\overline{u_k u_i u_j} + (2/3)\delta_{ij}\overline{u_k \partial_k p})/\rho \\
& && \text{turbulent transport}
\end{aligned}\right\} \tag{8}$$

On the assumption that $\rho' \ll \rho$ the overbar has been dropped from the mean density.

Aside from $\mathcal{P}$, the precise definition of the quantities in (8) is usually of minor importance. Their relevant properties are that ε is nonnegative, $\wp_{ij}$ is trace free, and T_{ij} is the divergence of a third-order tensor (if u_i is solenoidal). Obviously, (7) is not a closed equation for the second moment.

The equation for turbulent kinetic energy per unit mass is one-half of the trace of (7):

$$\partial_t k + U_j \partial_j k = \mathcal{P} - \varepsilon - \frac{1}{\rho}\left[\partial_j\left(\overline{u_j p} + \frac{1}{2}\rho\overline{u_j u_i u_i}\right) + \partial_i(\mu\partial_i k)\right] \tag{9}$$

where $k \equiv 1/2\overline{u_i u_i}$. Its rate of production is $\mathcal{P} \equiv 1/2\mathcal{P}_{ij} = -\overline{u_i u_k}\partial_k U_i$ and its rate of dissipation is ε.

The primary objective of turbulence modeling is to close the mean flow equation (6). Various formulations have been proposed in the course of time. Here we will only survey methods that add auxiliary transport equations; these are the sort used in general purpose computational fluid dynamics (CFD) codes. The closure schemes will be categorized into those based on transport of scalars and those based on transport of the Reynolds stress tensor. The first category includes single equations for eddy viscosity and pairs of equations for turbulent kinetic energy and its dissipation; the second category consists of methods based on the Reynolds stress transport equation (7).

3 MODELS WITH SCALAR VARIABLES

The purpose of closure models is to formulate a soluble set of equations to predict turbulence statistics. These consist of exact equations, such as (6), (7), and (9) plus formulas, or auxiliary equations, that express unclosed terms as functions of their dependent variables. The extra formulas must contain empiricism, often via a fairly small number of experimentally determined model constants, although sometimes empirical functions are also introduced to fit experimental curves. Unfortunately, the empiricism is not universal. There is a degree of freedom in which data are used to set the constants. On the other hand, closure models enable one to predict statistics of the very complex phenomenon of turbulent flow by solving a relatively simple set of equations. If no empirical constants were required, the implication would be that the closure represented either exact laws of fluid dynamics, or a systematically derived approximation. That degree of exactitude is impossible in predictive models for engineering flows.

The models discussed in this section have scalar dependent variables. Their basic purpose is to predict an eddy viscosity.

3.1 The $k - \varepsilon$ model

In part, $k - \varepsilon$ is popular for historical reasons: it was the first two-equation model used in applied CFD. However, it is not the only model available. Indeed, other models may be more accurate, or more computationally robust in many cases. Gradually, these other models are gaining wider usage. This chapter reviews several of them. It is inevitable that as the applications of CFD grow, further models will be developed and existing models will be adapted to particular needs. Closure modeling is an open-ended field that fills a critical need. What is now called the "standard" form for $k - \varepsilon$ is that developed by Jones and Launder (1972), with values for the empirical constants given by Launder and Sharma (1974). Although an enormous number of variations on the $k - \varepsilon$ model have been proposed, the standard model contains the essential elements, with the caveat that some form of fix is needed near to solid boundaries –as will be discussed later.

The $k - \varepsilon$ formula for eddy viscosity could be rationalized as follows. In parallel shear flow, the Reynolds shear stress

is assumed to be related to the velocity gradient by $-\overline{uv} = \nu_T \partial_y U$. Suppose that dissipation and production of turbulent energy are approximately in balance, $\varepsilon \approx \mathcal{P}$, where $\mathcal{P} = -\overline{u_i u_j}\partial_i U_j$ (equation 8). In parallel shear flow, $\mathcal{P} = -\overline{uv}\partial_y U$. Multiplying $\varepsilon \approx \mathcal{P}$ by ν_T gives

$$\nu_T \varepsilon \approx \nu_T \mathcal{P} = \nu_T(-\overline{uv}\partial_y U) = (\overline{uv})^2 \approx 0.09k^2 \tag{10}$$

upon invoking the experimental observation that $\overline{uv}/k \approx 0.3$ in many equilibrium shear layers (Townsend, 1976). Rearranging the above, $\nu_T \approx 0.09k^2/\varepsilon$. This formula is usually written

$$\nu_T = \frac{C_\mu k^2}{\varepsilon} \tag{11}$$

and the standard value of C_μ is 0.09.

Alternatively, it can simply be argued by dimensional analysis that the turbulence correlation time scale is $T \sim k/\varepsilon$ and the velocity scale squared is k. Then by the formula, $\nu_T \sim u^2 T$ derived by Taylor (1921), $\nu_T \sim C_\mu k^2/\varepsilon$. By either rationale, one sees that formulas to parameterize turbulent mixing can be evaluated from a model that predicts k and ε.

The mean flow (6) is computed with the scalar eddy viscosity and the constitutive relation

$$-\overline{u_i u_j} = 2\nu_T\left(S_{ij} - \frac{1}{3}\delta_{ij}S_{kk}\right) - \frac{2}{3}k\delta_{ij} \tag{12}$$

where S_{ij} is the mean rate of strain tensor $(1/2)(\partial_i U_j + \partial_j U_i)$. Substituting the constitutive model (12) closes the mean flow equation (6). The constitutive equation (12) is a linear stress–strain relation, as for a Newtonian fluid; nonlinear models also have been proposed at times (Section 3.7). The problem addressed by the $k-\varepsilon$ transport model is how to robustly predict ν_T. The formula (11) reduces this to: predict the spatial and temporal distribution of k and ε.

Equation (9), is the exact, but unclosed, evolution equation for k. To "close" it, the transport and pressure diffusion terms together are replaced by a gradient transport model:

$$-\partial_j\left(\frac{1}{2}\rho\overline{u_j u_i u_i}\right) - \partial_j(\overline{u_j p}) \approx \partial_j\left(\frac{\mu_T}{\sigma_k}\partial_j k\right) \tag{13}$$

This is based on a notion that the third velocity moment represents random convection of turbulent kinetic energy, that pressure–velocity correlation diffuses momentum, and that these can be replaced by gradient transport. The transport equation for k, with (13) substituted is

$$\partial_t k + U_j\partial_j k = \mathcal{P} - \varepsilon + \frac{1}{\rho}\partial_j\left[\left(\mu + \frac{\mu_T}{\sigma_k}\right)\partial_j k\right] \tag{14}$$

The usual value of σ_k is 1. Note that $\mathcal{P} \equiv -\overline{u_i u_j}S_{ij}$. Then, with (12)

$$\begin{aligned}\mathcal{P} &= 2\nu_T S_{ij}S_{ji} - \frac{2}{3}k\partial_i U_i - \frac{2}{3}\nu_T(\partial_i U_i)^2 \\ &= 2\nu_T|S|^2 - \frac{2}{3}k\,\boldsymbol{\nabla}\cdot\boldsymbol{U} - \frac{2}{3}\nu_T(\boldsymbol{\nabla}\cdot\boldsymbol{U})^2\end{aligned}$$

For incompressible mean flow, this reduces to $\mathcal{P} = 2\nu_T|S|^2$.

The modeled transport equation for ε cannot be derived systematically. Essentially it is a dimensionally consistent analogy to the above k-equation:

$$\partial_t\varepsilon + U_j\partial_j\varepsilon = \frac{C_{\varepsilon 1}\mathcal{P} - C_{\varepsilon 2}\varepsilon}{T} + \frac{1}{\rho}\partial_j\left[\left(\mu + \frac{\mu_T}{\sigma_\varepsilon}\right)\partial_j\varepsilon\right] \tag{15}$$

The time scale $T = k/\varepsilon$ makes it dimensionally consistent. Equation (15) is analogous to (14), except that empirical constants $C_{\varepsilon 1}$, $C_{\varepsilon 2}$, and σ_ε have been added because the ε-equation is just an assumed form. The terms on the right side can be referred to as *production of dissipation*, *dissipation of dissipation*, and *diffusion of dissipation*. The empirical coefficients are chosen in order to impose certain experimental constraints. The standard values for the constants are (Launder and Sharma, 1974)

$$C_\mu = 0.09;\quad C_{\varepsilon 1} = 1.44;\quad C_{\varepsilon 2} = 1.92;\quad \sigma_\varepsilon = 1.3 \tag{16}$$

These constants were chosen some time ago. More recent data suggest that slightly different values might be suitable, but the standard constants give reasonable engineering results in many situations. It is not likely that minor adjustments would significantly affect the predictive accuracy.

$C_{\varepsilon 1}$ is a critical constant. It controls the growth rate of shear layers: a 7% decrease of $C_{\varepsilon 1}$ increases the spreading rate by about 25%. This is a bit misleading, because the spreading rate is determined by $C_{\varepsilon 1} - 1$, so the leading 1 is irrelevant and the change in spreading rate is nearly proportionate to $C_{\varepsilon 1} - 1$. The standard value of $C_{\varepsilon 1}$ was chosen to fit the spreading rate of a plane mixing layer. Slightly different values would be obtained for other flows.

Very briefly, $C_{\varepsilon 2}$ is determined by the decay exponent measured in grid turbulence: if $k \sim t^{-n}$ then $C_{\varepsilon 2} = 1 + 1/n$ (Typical data would give $C_{\varepsilon 2} \approx 1.83$.) The value of C_μ has been discussed previously.

The $k-\varepsilon$ model has an important closed form solution in the log-layer. In this layer $\partial_y U = u_*/\kappa y$, where $u_* = \sqrt{(\tau_w/\rho)}$, with τ_w being the wall shear stress and κ is the VonKarman constant. One finds that (Durbin and Reif, 2010; Wilcox, 1998)

$$\left.\begin{aligned}\mathcal{P} = \varepsilon &= \tfrac{u_*^3}{\kappa y} \\ \nu_T &= \kappa u_* y \\ k &= \tfrac{u_*^2}{\sqrt{C_\mu}}\end{aligned}\right\} \tag{17}$$

This solution provides the value of σ_ε

$$\sigma_\varepsilon = \frac{C_{\varepsilon 2} - C_{\varepsilon 1}}{\kappa^2 \sqrt{C_\mu}} \tag{18}$$

Measurements of κ are mostly in the range 0.41 ± 0.02. The standard value $\sigma_\varepsilon = 1.3$ corresponds to the high end of these measurements.

Although this log-layer solution plays a role in computational use of $k-\varepsilon$, the solution for k does not agree with experiments. Older data suggested that $k \sim 3.3u_*^2$ and hence that $C_\mu = 0.09$ in (17). Experiments by DeGraaff and Eaton (2000) question the correctness of these older data. The momentum thickness Reynolds number must be on the order of $R_\theta \approx 8000$, before a zone of constant k/u_*^2 is seen. However, that value increases with R_θ, which would imply that C_μ declines to values significantly lower than 0.09. While that certainly is of concern, it is not devastating: the log-layer eddy viscosity is predicted to be $\kappa u_* y$, which agrees quite well with data. Therefore, mean flow predictions do not fail. Presumably, the apparent Reynolds number dependence of C_μ would be counteracted by Reynolds number dependence of other coefficients, with little effect on mean flow prediction.

3.2 Boundary conditions and near-wall modifications

The boundary conditions to the $k-\varepsilon$ model at a no-slip wall are quite natural, but the near-wall behavior of the model is not. This is rather a serious issue in RANS computation. A variety of patches have been proposed in the course of time.

At a no-slip surface $\boldsymbol{u} = 0$, so $k = \overline{|\boldsymbol{u}|^2}/2$ has a quadratic zero. Hence both k and its normal derivative vanish. The natural boundary condition is

$$k = 0; \;\; \partial_n k = 0 \tag{19}$$

where $\partial_n \equiv \hat{\boldsymbol{n}} \cdot \boldsymbol{\nabla}$ is the derivative in the wall-normal direction. Equation (19) specifies two conditions on k and none on ε. That suffices to solve the coupled $k-\varepsilon$ system. However, in segregated equation algorithms, it is common practice to convert these into $k = 0$ and a condition on ε. As the wall is approached, (14) has the limiting behavior

$$\varepsilon_w = \nu \partial_y^2 k \tag{20}$$

Integrating (20) gives $k \to A + By + \varepsilon_w y^2/2\nu$, where A and B are integration constants. By (19) $A = B = 0$, so the wall value of dissipation is

$$\varepsilon_w = \lim_{y \to 0} \frac{2\nu k}{y^2} \tag{21}$$

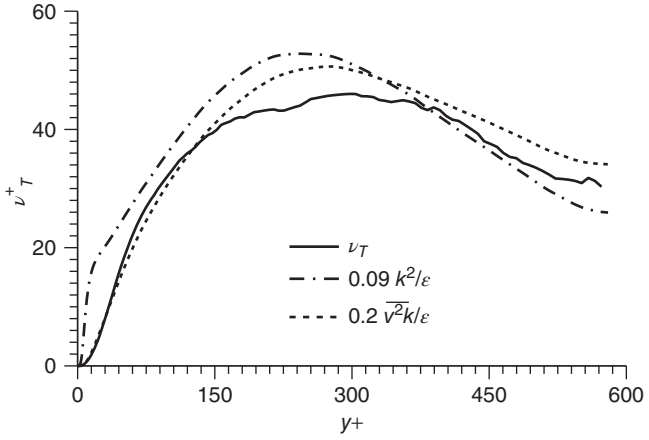

Figure 2. Exact eddy viscosity compared to the $k-\varepsilon$ and v^2-f formulas in channel flow at $R_\tau = 590$. Curves were computed from DNS data of Moser *et al*. (1999).

In CFD codes this, or something equivalent, is often used to impose the no-slip condition (19).

Unfortunately, deriving the correct no-slip boundary conditions is not the only issue in near-wall modeling. A second need is to prevent a singularity in the ε-equation (15). If the time scale $T = k/\varepsilon$ is used, then $T \to O(y^2)$ as $y \to 0$, and the right side of (15) becomes singular like ε^2/k. The Kolmogoroff scale, $\sqrt{(\nu/\varepsilon)}$, is an appropriate time scale near the surface. The formula (Durbin, 1991)

$$T = \max\left(\frac{k}{\varepsilon}, 6\sqrt{\frac{\nu}{\varepsilon}}\right) \tag{22}$$

can be used. The coefficient of 6 in formula (22) is an empirical constant. Several other methods that help avoid a singularity in the ε equation are discussed in Patel *et al*. (1984).

But the near-wall failure of standard $k-\varepsilon$ goes further. The formula $\nu_T = C_\mu k^2/\varepsilon$ gives an erroneous profile of eddy viscosity even if exact values of $k(y)$ and $\varepsilon(y)$ are known. The solid line in Figure 2 is the viscosity constructed from DNS data (Moser *et al*., 1999) by evaluating the exact definition $\nu_T^+ = -\overline{uv}/\nu d_y U$. It is compared to curves constructed by substituting the exact k and ε into the $k-\varepsilon$ formula (11). The model formula is seen to be grossly in error below $y_+ \approx 50$. Overpredicting the eddy viscosity in this region will greatly overpredict skin friction on the surface.

One device to fix (11) consists of "damping" the viscosity: to this end, it is replaced by

$$\nu_T = \frac{f_\mu C_\mu k^2}{\varepsilon} \tag{23}$$

In the literature the damping function, f_μ, has been made dependent either on ky/ν or on $k^2/\varepsilon\nu$, depending on the model. For example, Launder and Sharma (1974) used

$$f_\mu = \exp\left[\frac{-3.4}{(1+R_T/50)^2}\right]; \quad R_t = \frac{k^2}{\varepsilon\nu} \tag{24}$$

The reader might consult Patel *et al*. (1984) for tabulations of various other "low Reynolds number $k-\varepsilon$" formulations.

It is not sufficient to simply damp the eddy viscosity; all low Reynolds number $k-\varepsilon$ models also modify the ε-equation in one way or another. Launder and Sharma (1974) replace it with

$$\partial_t\tilde{\varepsilon} + U_j\partial_j\tilde{\varepsilon} = \frac{\tilde{\varepsilon}}{k}(C_{\varepsilon 1}\mathcal{P} - f_2 C_{\varepsilon 2}\tilde{\varepsilon}) + \frac{1}{\rho}\partial_j\left[\left(\mu + \frac{\mu_T}{\sigma_\varepsilon}\right)\partial_j\tilde{\varepsilon}\right] + 2\nu\nu_T\left(\frac{\partial^2 U}{\partial y^2}\right)^2 \tag{25}$$

The dependent variable $\tilde{\varepsilon}$ is defined as $\varepsilon - \nu|\nabla k|^2/2k$. This is a device that causes $\tilde{\varepsilon}$ to be zero at the wall. Throughout the model, including the eddy viscosity formula (23), ε is replaced by $\tilde{\varepsilon}$. The last term on the right side of (25) is not coordinate independent, but it is only important near the surface, so $\hat{y}$ can be considered the wall normal direction. The blending function

$$f_2 = 1 - 0.3\exp\ (-R_t^2)$$

was also inserted in (25).

The benefits of adopting low Reynolds number $k-\varepsilon$ models in practical situations seem limited. Given the confusingly large number of the formulations, their numerical stiffness and their inaccurate predictions in flows with significant pressure gradient, they are not attractive for full RANS computation.

3.3 Two-layer models

A viable alternative to near-wall damping is to formulate a simplified model for the wall region, and to patch it onto the $k-\varepsilon$ model away from the wall. The $k-\ell$ formulation has been used to this end, in an approach called the *two layer* $k-\varepsilon$ *model* (Chen and Patel, 1998).

The $k-\ell$ model uses the k-equation (14), but replaces the ε-equation (15) by the algebraic formula

$$\varepsilon = \frac{k^{3/2}}{\ell_\varepsilon} \tag{26}$$

$$\ell_\varepsilon = C_\ell y\left(1 - \mathrm{e}^{-y\sqrt{k}/\nu A_\varepsilon}\right) \tag{27}$$

is obtained if $A_\varepsilon = 2C_\ell$. The eddy viscosity (11) will not have the right damping if (26) is substituted. Doing so would give $\nu_T = \sqrt{(k)}\,\ell_\varepsilon$. Therefore, a separate length is used in the formula

$$\nu_T = C_\mu\sqrt{k}\,\ell_\nu \tag{28}$$

$$\ell_\nu = C_\ell y\left(1 - \mathrm{e}^{-y\sqrt{k}/\nu A_\nu}\right) \tag{29}$$

The log-layer solution (17) then gives $C_\ell = \kappa/C_\mu^{3/4}$. Given the VonKarman constant $\kappa = 0.41$ and that C_μ retains its value 0.09, the only new empirical constant is A_ν. The value $A_\nu = 62.5$ gives a good fit to skin friction data in zero pressure gradient boundary layers.

The $k-\ell$ and $k-\varepsilon$ models are patched at some distance from the wall. Common practice is to do this, where $1 - \mathrm{e}^{-y\sqrt{(k)}/\nu A_\nu}$ reaches 0.95; this occurs at $y_{\mathrm{sw}} = \log(20)A_\nu\nu/\sqrt{(k(y_{\mathrm{sw}}))}$. Succinctly, the two-layer model solves the k-equation (14) at all points in the flow, but instead of (15) the ε-equation is represented by

$$\mathcal{L}[\varepsilon] = \mathcal{S} \tag{30}$$

The operator $\mathcal{L}$ and source $\mathcal{S}$ are defined as

$$\mathcal{L} = \begin{cases} \partial_t + U_j\partial_j - \frac{1}{\rho}\partial_j\left(\mu + \frac{\mu_T}{\sigma_\varepsilon}\right)\partial_j & y > y_{\mathrm{sw}} \\ 1 & y \le y_{\mathrm{sw}} \end{cases} \tag{31}$$

$$\mathcal{S} = \begin{cases} \frac{C_{\varepsilon 1}\mathcal{P} - C_{\varepsilon 2}\varepsilon}{T} & y > y_{\mathrm{sw}} \\ \frac{k^{3/2}}{\ell_\varepsilon} & y \le y_{\mathrm{sw}} \end{cases} \tag{32}$$

This two-layer formulation has proved effective in practical computations (Rodi, 1991) and usually gives better predictions than wall functions. But it does require a fine grid near to walls, and so is more expensive computationally than wall functions.

3.4 Wall functions

Another method that circumvents the erroneous predictions in the near-wall region is to abandon the $k-\varepsilon$ equations in a zone next to the wall and to impose boundary conditions at the top of that zone. Within the zone, the turbulence and mean velocity are assumed to follow prescribed profiles. This is the "wall function" method. Conceptually, the wall function is used in the law-of-the-wall region and the $k-\varepsilon$ model predicts the flow field farther from the surface. The two share the logarithmic layer as a common asymptote. They are patched together in that layer. Wall functions are used with models other than $k-\varepsilon$, as well, to reduce grid requirements.

Let d be the distance from the wall at which the patching is done. At that point the log-layer solution $\mathrm{d}U/\mathrm{d}y = u_*/\kappa d$, $k = u_*^2/\sqrt{(C_\mu)}$, and $\varepsilon = u_*^3/\kappa d$ (see equation 17) is assumed to be valid. This is an exact solution to the standard $k-\varepsilon$ model in a constant stress layer, so smooth matching is possible in principle; in practice, wall functions are used even when they are not mathematically justified, such as in a separating flow.

The friction velocity, u_*, is found by solving the implicit formula

$$U(d) = \frac{u_*}{\kappa} \ln\left(\frac{\mathrm{d}u_*}{\nu}\right) + B \tag{33}$$

with a typical value of $B = 5.1$. The tangential surface shear stress is assumed to be parallel to the direction of the mean velocity, and is $\tau_w = \rho u_*^2$ in magnitude. In a finite volume formulation τ_w provides the momentum flux on the wall face.

At a two-dimensional separation point, $u_* = 0$. To avoid problems as u_* changes sign, the boundary conditions can be expressed in terms of a different velocity scale, $u_k \equiv (k\sqrt{(C_\mu)})^{1/2}$. They then assume the form (Launder and Spalding, 1974)

$$\frac{\mathrm{d}U}{\mathrm{d}n} = \frac{\tau_w}{\rho\kappa u_k\, y_p}, \quad \varepsilon = \frac{u_k^3}{\kappa y_p}, \quad \frac{\mathrm{d}k}{\mathrm{d}n} = 0 \tag{34}$$

In practice, the conditions (34) are applied at the grid point closest to the solid boundary, $y(1)$; this point should be located above $y_+ \approx 40$ and below $y \approx 0.2\delta_{99}$, where δ_{99} is the 99% boundary layer thickness.

The wall function procedure is rationalized by appeal to the two-layer, law-of-the-wall/law-of-the-wake, boundary layer structure. The law-of-the-wall is assumed to be of a universal form, unaffected by pressure gradients or flow geometry. Its large y_+ asymptote, (34), is its only connection to the nonuniversal part of the flow field. Through this, the skin friction can respond to external forces. However, in highly perturbed flows the assumption of a universal wall layer is not consistent with experiments. Predictions made with wall functions then deteriorate.

As a practical matter, it is sometimes impossible to ensure that the first point of a computational grid lies in the log-layer, if a log-layer exists at all. It is not possible *a priori* to generate a computational mesh that will ensure that the first computational node is neither too close nor too far from the wall. Accurate computation may require *a posteriori* modification of the mesh to achieve a suitable y_+.

In complex flows, it is likely that the wall function will be used beyond its range of justifiability. On the other hand, wall functions can significantly reduce the cost of a CFD analysis. The steepest gradient of turbulent energy occurs near the wall ($y_+ \lesssim 10$). By starting the solution above this region, the computational stiffness is reduced. Because of this stiffness, the near-wall region requires a disproportionate number of grid points; avoiding it with a wall function reduces grid requirements. Wall functions therefore are widely used for engineering prediction.

Various methods have been proposed to extend the validity of wall functions to $y_+ \lesssim 40$ in the interest of more flexible meshing. In principle, the wall function boundary condition can be imposed anywhere in the law-of-the-wall region. For instance, a solution in that near-wall region can be tabulated and used as a boundary condition (Kalitzen *et al.*, 2005). Another approach is called a "scalable" wall function, which largely consists of replacing the non-dimensional wall distance by $\max(y^+, 11.2)$ (Vieser *et al.*, 2002).

3.5 The $k-\omega$ model

The eddy viscosity is of the form $\nu_T = C_\mu u^2 T$, where T is a correlation time. One role of the ε-equation is to provide this scale via $T = k/\varepsilon$. Instead, one might consider combining the k-equation directly with a time-scale equation. It turns out to be more suitable to use a quantity, ω, that has dimensions of inverse time. Then the eddy viscosity is represented as $\nu_T = k/\omega$.

The $k-\omega$ model of Wilcox (1998) can be written as

$$\begin{aligned}
\partial_t k + U_j\partial_j k &= 2\nu_T|S|^2 - C_\mu k\omega + \frac{1}{\rho}\partial_j\left[\left(\mu + \frac{\mu_T}{\sigma_k}\right)\partial_j k\right] \\
\partial_t \omega + U_j\partial_j \omega &= 2C_{\omega 1}|S|^2 - C_{\omega 2}\omega^2 + \frac{1}{\rho}\partial_j\left[\left(\mu + \frac{\mu_T}{\sigma_\omega}\right)\partial_j \omega\right] \\
\nu_T &= \frac{k}{\omega}
\end{aligned} \tag{35}$$

The k-equation is altered only by changing ε to $k\omega$. The ω-equation is quite analogous to the ε-equation. The standard constants are $C_{\omega 1} = 5/9$, $C_{\omega 2} = 3/40$, $\sigma_\omega = \sigma_k = 2$, and $C_\mu = 0.09$.

Figure 3 shows the near-wall behavior of a solution to the $k-\omega$ model in plane channel flow with $R_\tau = 590$. The profile of $\varepsilon = C_\mu k\omega$ has been multiplied by 50 for display. The region next to the wall is critical to heat and momentum exchange between the fluid and the surface. In the wall layer, the $k-\omega$ predictions of k and ε are at odds with the data. ε erroneously goes to zero at the surface and has a spurious peak near $y_+ = 10$. The consequence of the spurious peak is that k is excessively dissipated near the wall. While these erroneous predictions might at first be disconcerting, in fact the underestimation of k and overestimation of ε are exactly what are needed to counter the overprediction of ν_T displayed by the formula $C_\mu k^2/\varepsilon$ in Figure 2. Both of these features contribute to giving ν_T a more reasonable

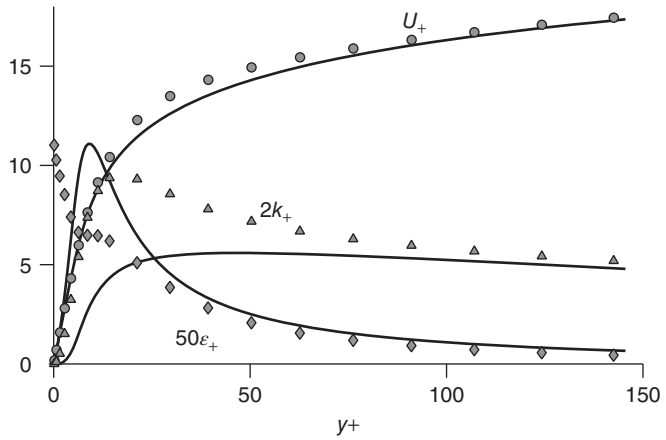

Figure 3. Channel flow solution to $k-\omega$. The centerline is at $y+=590$. The curves are solutions to the model. ● are DNS data for U; ▲ are data for $2k$; and ♦ are for 50ε.

distribution. Indeed, the U predictions in Figure 3 agree quite well with data, given that no wall corrections have been made to the model. $k-\omega$ is usable near boundaries, without wall functions or wall damping – that is its remarkable property.

Near a no-slip surface equations (35) have the limiting solution $\omega_+ = 6/(C_{\omega 2} y_+^2)$, and $k \propto y_+^m$ with $m = (1/2) + \sqrt{(149/20)} = 3.23$. This shows that ω is singular at no-slip boundaries. Nonsingular solutions also exist; Wilcox (1998) proposed that wall roughness could be represented by prescribing a finite boundary value for ω. However, on smooth walls the singular solution is usually invoked.

3.5.1 The SST variant

Menter (1992) noted two failings of the basic $k-\omega$ model, one minor and one major. The former is that it overpredicts the level of shear stress in adverse pressure gradient boundary layers. The latter is its spurious sensitivity to free-stream conditions: the spreading rate of free shear flows shows an unphysical dependence on the free-stream value of ω.

To overcome the shortcomings of the basic $k-\omega$ model, Menter proposed the "shear stress transport" (SST) model. This variant of $k-\omega$ has been found quite effective in predicting many aeronautical flows. To limit the Reynolds shear stress in strong pressure gradients, Menter introduced the bound

$$\nu_T = \min\left[\frac{k}{\omega}, \frac{\sqrt{C_\mu}k}{|2\mathbf{\Omega}|F_2}\right] \tag{36}$$

where

$$\Omega_{ij} \equiv \frac{1}{2}\left(\partial_i U_j - \partial_j U_i\right) \tag{37}$$

and $|\mathbf{\Omega}|$ is its magnitude.

Formula (36) is an unwanted constraint in free shear flow. The limiter is confined to the boundary layer by the blending function

$$\begin{aligned} F_2 &= \tan\ h(\arg_2^2) \\ \arg_2 &= \max\left[\frac{2\sqrt{k}}{C_\mu \omega y}, \frac{500\nu}{\omega y^2}\right] \end{aligned} \tag{38}$$

The blending function (38) is devised so that F_2 is nearly unity in most of the boundary layer, dropping to zero near the top and in the free-stream. F_2 multiplies the second term in the *min* function of equation (36).

To rectify the spurious free-stream sensitivity of the original $k-\omega$ model, Menter developed a two zone formulation that uses $k-\omega$ near the wall and $k-\varepsilon$ for the rest of the flow. The switch between these forms is by a smooth interpolation. Now the blending function is

$$\begin{aligned} F_1 &= \tan\ h(\arg_1^4) \\ \arg_1 &= \min\left[\max\left(\frac{\sqrt{k}}{C_\mu \omega y}, \frac{500\nu}{\omega y^2}\right), \right. \\ &\qquad \left. \frac{2k\omega}{y^2 \max(\nabla k \cdot \nabla \omega, 10^{-20})}\right] \end{aligned} \tag{39}$$

This seemingly intricate function is simply an operational device to interpolate between the $k-\omega$ and $k-\varepsilon$ models. F_1 is devised to be near unity in the inner half of the boundary layer and to decrease through the outer half, dropping to zero slightly inside its top edge.

The term

$$S_\omega = \frac{2}{T}\left(\nu + \frac{\nu_T}{\sigma_\omega}\right)\left[\frac{|\nabla k|^2}{k} - \frac{\nabla k \cdot \nabla \varepsilon}{\varepsilon}\right]$$

which arises when the exchange $\omega \to \varepsilon/k$ is used to transform the ω-equation into the ε-equation, is faded out via F_1:

$$\partial_t \varepsilon + U_j \partial_j \varepsilon = \frac{C_{\varepsilon 1}\mathcal{P} - C_{\varepsilon 2}\varepsilon}{T} + \partial_j\left[\left(\nu + \frac{\nu_T}{\sigma_\varepsilon}\right)\partial_j \varepsilon\right] + F_1 S_\omega \tag{40}$$

Thereby a transition between the ε and ω equations typically is brought about across the middle of the boundary layer. To complete this formulation, the model constants also are interpolated as

$$\begin{aligned} C_{\varepsilon 1} &= 1 + (1 - F_1)0.44 + F_1 C_{\omega 1} \\ C_{\varepsilon 2} &= 1 + (1 - F_1)0.92 + F_1 C_{\omega 2} \end{aligned}$$

These provide the $k-\varepsilon$ values when $F_1 = 0$ and the $k-\omega$ values when $F_1 = 1$. The coefficients σ_k and σ_ε are interpolated similarly.

A simpler method for avoiding free-stream sensitivity is to add a cross-diffusion term to (35) (Wilcox, 1998, Kok, 2000):

$$\partial_t\omega + U_j\partial_j\omega = 2C_{\omega1}|S|^2 - C_{\omega2}\omega^2 + \frac{1}{\rho}\partial_j\left[\left(\mu + \frac{\mu_T}{\sigma_\omega}\right)\partial_j\omega\right] + \frac{\sigma_d}{\omega}\max\{\boldsymbol{\nabla} k\cdot\nabla\omega, 0\} \tag{41}$$

Kok (2000) suggests the values σ_d, $\sigma_k = 1.5$, $\sigma_\omega = 2$.

3.5.2 The large strain rate anomaly

The large strain rate anomaly is that excessive levels of turbulent kinetic energy are predicted by standard two-equation models in regions of large mean rate of strain. The following reviews two ideas to solve this problem.

In nondivergent flow the rate of production of turbulent energy is $\mathcal{P} = 2\nu_t|S|^2$. Launder and Kato (1993) attribute excessive levels of k to an overestimate of $\mathcal{P}$ in pure straining flow. As a pragmatic device to avoid the problem of spurious stagnation point build-up of turbulent kinetic energy, they replaced $|S|^2$ with $|S||\Omega|$, where Ω_{ij} is defined by (37) and $|\Omega|^2 = \Omega_{ij}\Omega_{ij}$. Hence the rate of production is zero in irrotational flow ($|\Omega| = 0$). This is the first idea for avoiding the large rate of strain anomaly.

The second idea is to invoke a time-scale bound. The eddy viscosity predicted by scalar equation turbulence models can be characterized by the form

$$\mu_t = C_\mu\rho u^2 T \tag{42}$$

where u is the velocity scale and T is the turbulence time scale. In $k-\varepsilon$ and $k-\omega$ models, $u^2 = k$. T equals k/ε, in $k-\varepsilon$, and it equals $1/\omega$ in $k-\omega$. Note that T also appears in the source term $(C_{\varepsilon1}\mathcal{P} - C_{\varepsilon2}\varepsilon)/T$ of the ε-equation and that production of turbulent energy can be stated as $\mathcal{P} = 2C_\mu k|S|^2 T$.

A bound for the turbulent time scale T can be derived (Durbin and Reif, 2010) from the condition that the eigenvalues of the Reynolds stress tensor as estimated by formula (12) should be nonnegative:

$$T = \min\left[\frac{k}{\varepsilon}, \frac{\alpha}{\sqrt{6}C_\mu|S|}\right]$$

or

$$T = \min\left[\frac{1}{C_\mu\omega}, \frac{\alpha}{\sqrt{6}C_\mu|S|}\right] \tag{43}$$

The eigenvalue bound is invoked by introducing the constant $\alpha \le 1$. For compressible flows, S should be replaced by $S^* = S - (1/3)(\nabla\cdot U)I$. The value $\alpha = 0.6$ was selected.

3.6 Eddy viscosity transport models

Two equation models construct an eddy viscosity from velocity and time scales. It might seem prudent instead to formulate a transport equation directly for the eddy viscosity. That idea was initiated by Baldwin and Barth (1990) and improved upon by Spalart and Allmaras (1992) to produce the model described here. The Spalart–Allmaras (S–A) model enjoyed initial success in predicting aerodynamic flows and is now established for general flows.

Assume *a priori* that an effective viscosity, $\tilde{\nu}$, satisfies a prototype transport equation

$$\partial_t\tilde{\nu} + \boldsymbol{U}\cdot\boldsymbol{\nabla}\tilde{\nu} = \mathcal{P}_\nu - \varepsilon_\nu + \frac{1}{\sigma_\nu}\left[\boldsymbol{\nabla}((\nu+\tilde{\nu})\boldsymbol{\nabla}\tilde{\nu}) + c_{b2}|\boldsymbol{\nabla}\tilde{\nu}|^2\right] \tag{44}$$

Aside from the term multiplying c_{b2} this is analogous to the k, ε, or ω equations: the right side consists of production, destruction, and transport. The c_{b2} term is added to control the evolution of free shear layers. This equation has a propagating front solution, with the propagation speed depending on c_{b2}. Spalart and Allmaras (1992) argue that the front speed influences shear layer development, and choose $c_{b2} = 0.622$, in conjunction with $\sigma_\nu = 2/3$, to obtain a good representation of the velocity profiles in wakes and mixing layers.

The cleverness in developing an equation for an effective viscosity, $\tilde{\nu}$, rather than the actual eddy viscosity, ν_T, is that a numerical amenity can be added. Baldwin and Barth (1990) proposed to make $\tilde{\nu}$ vary linearly throughout the law-of-the-wall layer, in particular, to nearly retain the log-layer dependence $\tilde{\nu} = \kappa u_* y$ all the way to the wall.

For production, choose the dimensionally consistent form

$$\mathcal{P}_\nu = c_{b1}|2\tilde{\Omega}| \tag{45}$$

Spalart and Allmaras selected the constant to be $c_{b1} = 0.1355$. The wall distance d is used for a length scale in the destruction term

$$\varepsilon_\nu = f_w c_{w1}\left(\frac{\tilde{\nu}}{d}\right)^2$$

The function f_w is discussed below. The expression $c_{w1} = c_{b1}\kappa^{-2} + (1+c_{b2})/\sigma_\nu$ can be derived from log-layer scaling.

The intriguing part is that $\tilde{\nu}$ is contrived to vary nearly linearly all the way to the wall, in theory. This is achieved by deriving the formula

$$|\tilde{\Omega}| = |\Omega| - \frac{\tilde{\nu}^2}{(\nu_T+\nu)(\kappa y)^2} + \frac{\tilde{\nu}}{(\kappa y)^2} \tag{46}$$

for the effective vorticity in (45). Next to a wall, the second factor on the right cancels $|\Omega|$ and the third provides $|\tilde{\Omega}|$, leading to the desired behavior of $\tilde{\nu}$ – in consequence of $|\tilde{\Omega}| \propto (1/y)$.

A formulation with a nearly linear solution near the wall is attractive; but the real eddy viscosity is *not* linear near the wall. This is rectified by a nonlinear transformation: let

$$\nu_T = \tilde{\nu} f_v \left(\frac{\tilde{\nu}}{\nu} \right) \tag{47}$$

The transforming function

$$f_v \left(\frac{\tilde{\nu}}{\nu} \right) = \frac{(\tilde{\nu}/\nu)^3}{(\tilde{\nu}/\nu)^3 + 7.1^3}$$

was adopted by Spalart and Allmaras (1992).

The function f_w in front of the destruction term remains to be specified. That function implements a constraint that, far from the surface, the wall distance should drop out of the model. The particular form has an arbitrary appearance; it is

$$f_w(r) = g\left[\frac{65}{g^6 + 64}\right]^{1/6}, \quad \text{with} \quad g = r + 0.3(r^6 - r)$$
$$\text{and} \quad r \equiv \frac{\tilde{\nu}}{\tilde{\Omega}(\kappa d)^2} \tag{48}$$

Formula (48) was selected to provide accurate agreement with experimental data on skin friction beneath a flat plate boundary layer.

3.7 Nonlinear constitutive equations

Eddy viscosity models usually invoke the quasilinear stress – strain rate relation (12). There are obvious shortcomings to that formula: for instance, it incorrectly predicts that the *normal* stresses are isotropic in parallel shear flow: $\overline{u^2} = \overline{v^2} = \overline{w^2} = (2/3)k$ when U is a function only of y. To a large extent one hopes that (12) will adequately represent the *shear* stresses, as these are often dominant in the mean momentum equation. However, the normal stresses generally will not be correct, even qualitatively.

An elaborate correction to some shortcomings of eddy viscosity is provided by RST models. Stress transport models will be discussed in Section 4. An intermediate level of modeling would seem to be provided by nonlinear, but still algebraic, constitutive formulas. In practice, it remains unclear what level of improved prediction nonlinear constitutive models provide. They promise to add physical effects that are not accommodated by the linear formula. For instance, the normal stresses in parallel shear flow can be unequal and the Reynolds stress can become dependent on system rotation. However, it should be warned that nonlinear constitutive models tend to increase numerical stiffness.

One postulates that $\overline{u_i u_j}$ is a tensor function of the rate of strain $\boldsymbol{S}$ and the rate of rotation $\boldsymbol{\Omega}$, as well as of the scalar quantities k and ε. What are the constraints on the possible functional form? The principle of material frame indifference would demand that *material properties* be independent of the rate of rotation, but *turbulent stresses* are most definitely affected by rotation. This is because they are not material properties but properties of the flow. So the only constraints are that the formula must be tensorally and dimensionally consistent. Our discussion is further simplified by restricting it to two-dimensional mean flow.

Let the stress tensor be a function of two trace-free tensors: $\overline{u_i u_j} = \mathcal{F}_{ij}(\boldsymbol{\Omega}, \boldsymbol{S})$. By the extended Cayley – Hamilton theorem (Goodbody, 1982), in two dimensions, the most general isotropic function can depend tensorally on $\boldsymbol{I}$, $\boldsymbol{S}$, $\boldsymbol{\Omega}$, and $\boldsymbol{S}^2$, where the last is used in place of the two-dimensional identity tensor. It can also depend on products of these; but, it can be shown that the only tensorally independent product is $\boldsymbol{S} \cdot \boldsymbol{\Omega}$ (Pope, 1975).

The most general constitutive model for three velocity-component turbulent stresses in a two-dimensional, incompressible mean flow is provided by

$$-\overline{\boldsymbol{u}\boldsymbol{u}} = C_{\tau_1} kT\boldsymbol{S} - \frac{2}{3}k\boldsymbol{I} + kT^2 \left[C_{\tau_2} (\boldsymbol{S} \cdot \boldsymbol{\Omega} - \boldsymbol{\Omega} \cdot \boldsymbol{S}) + C_{\tau_3} \left(\boldsymbol{S}^2 - \frac{1}{3}\text{trace}(\boldsymbol{S}^2)\boldsymbol{I} \right) \right] \tag{49}$$

where T is a turbulence time scale (e.g., k/ε). The linear model is $C_{\tau_1} = C_\mu$ and $C_{\tau_2} = 0 = C_{\tau_3}$. In nonlinear models these coefficients can be made functions of the invariants $|\boldsymbol{S}|^2 T^2$ and $|\boldsymbol{\Omega}|^2 T^2$. One method to derive the functional dependence is by solving an equilibrium approximation to one of the RST equations, as discussed in Section 4.3 (Gatski and Speziale, 1993). Another method is simply to postulate forms for the coefficients, instances of which are described by Apsley and Leschziner (1999).

In three dimensions, a number of further terms are needed to obtain the most general tensor representation. Several authors have explored truncated versions of the general three-dimensional form. Craft *et al.* (1999) explored a version that includes terms cubic in $\boldsymbol{S}$, $\boldsymbol{\Omega}$, and their products. Craft *et al.* (1999) also discuss methods to accelerate numerical convergence of the RANS equations with nonlinear constitutive models. These methods are of the variety described in Section 5.1: essentially, an effective viscosity is extracted and included with the viscous term, and dissipative source terms are treated implicitly in the k and ε equations.

4 SECOND MOMENT TRANSPORT

Anisotropy exists in all real flows. In parallel shear flows, the dominant anisotropy is the shear stress. Eddy viscosity models are designed to represent shear stress; they are not designed to represent normal stress anisotropy. Second moment closure (SMC) is based on transport equations for the entire stress tensor.

The limitations to scalar models stem largely from the turbulence being represented by its kinetic energy, which is a scalar, and from the eddy viscosity assumption (12). The former does not correctly represent turbulence anisotropy; the latter assumes an instantaneous equilibrium between the Reynolds stress tensor and the mean rate of strain. A shortcoming in representing the turbulent velocity fluctuations solely by the scalar magnitude k is that sometimes an external force acts on one component more strongly than others. For example, stable streamline curvature will suppress the component directed toward the center of curvature. Another shortcoming in the eddy viscosity representation is that it causes the Reynolds stresses to change instantaneously with the mean rate of strain. Disequilibrium should come into play in rapidly changing flow conditions. SMC incorporates many of these effects in a natural way because it is based on the RST equations (7). For instance, curvature appears in the production tensor $\mathcal{P}_{ij}$. The price paid for the increased physical content of the model is that more equations must be solved. Hanjalic (1994) discusses further pros and cons in developing models for the transport of Reynolds stresses.

The essence of SMC modeling can be described by reference to homogeneous turbulence. Our discussion begins there. Under the condition of homogeneity the exact transport equation (7) takes the form

$$\partial_t \overline{u_i u_j} = \mathcal{P}_{ij} + \wp_{ij} - \frac{2}{3}\varepsilon\delta_{ij} \tag{50}$$

Note that ε is the dissipation rate of k so that $\varepsilon \equiv (1/2)\varepsilon_{ii}$. Indeed, the trace of (50) is two times the k equation. In that sense, SMC modeling can be looked on as unfolding the $k-\varepsilon$ model to recover a better representation of stress anisotropy.

The explicit form for the production tensor is stated below (7) to be

$$\mathcal{P}_{ij} = -\overline{u_j u}_k \partial_k U_i - \overline{u_i u}_k \partial_k U_j$$

which involves the dependent variable $\overline{u_i u_j}$ and the mean flow gradients. The only new unclosed term in (50) is redistribution, $\wp_{ij}$, assuming either that the ε-equation (15) or the ω-equation (41) is retained.

Modeling involves developing formulas and equations to relate the unclosed term to the mean flow gradients and to the dependent variable, $\overline{u_i u_j}$. What is needed is a tensor function of tensors,

$$\wp_{ij} = F_{ij}(\overline{u_i u_j}, \partial_j U_i, \delta_{ij}; k, \varepsilon)$$

It is common to nondimensionalize $\overline{u_i u_j}$ by k and subtract $(2/3)\delta_{ij}$ to form a trace-free, anisotropy tensor

$$b_{ij} \equiv \frac{\overline{u_i u_j}}{k} - \frac{2}{3}\delta_{ij} \tag{51}$$

$$\wp_{ij} = \varepsilon \mathcal{F}_{ij}\left[b_{ij}, \frac{k}{\varepsilon}\partial_j U_i, \delta_{ij}\right] \tag{52}$$

in the present case of homogeneous flow. The functional form is local in time: in particular, $\mathcal{F}$ could be a functional of $b_{ij}(t')$, $t' \le t$. However, all SMC models currently in use invoke a temporally local redistribution model; all variables in (52) are evaluated at the same time t. History effects are present, but only through the evolution equation (50).

Common practice is to separate $\wp$ into slow and rapid contributions, $\wp^{\text{slow}} + \wp^{\text{rapid}}$, and to model their functional dependence, $\mathcal{F}^{\text{slow}} + \mathcal{F}^{\text{rapid}}$, separately. Terms that do not depend on $\partial_j U_i$ are referred to as the *slow terms* of the redistribution model. The rapid terms depend on velocity gradients; they are usually tensorally linear in $\partial_j U_i$.

4.1 Models for the slow part

The slow term is associated with the problem of return to isotropy. To isolate slow terms, consider the case $\partial_j U_i = 0$. Then there is no directional preference imposed on the turbulence and hence no driving force toward anisotropy. In that case (52) becomes $\wp_{ij} = \varepsilon \mathcal{F}_{ij}[\boldsymbol{b}, \boldsymbol{\delta}]$. The most commonly used form for slow redistribution is the *Rotta model*

$$\wp_{ij}^{\text{slow}} = -C_1 \varepsilon b_{ij} \tag{53}$$

with b_{ij} toward 0, or of $\overline{u_i u_j}$ toward $(2/3)k\delta_{ij}$. For that reason it is called a return to isotropy model. Typical empirical values of C_1 are in the range 1.5–2.0. The concept that the slow term produces a tendency toward isotropy demands that $C_1 > 1$ (Durbin and Reif, 2010).

The Rotta model is usually quite effective. However, the Cayley–Hamilton theorem shows that the most general functional dependence of the slow redistribution model is

$$\wp_{ij}^{\text{slow}} = -\varepsilon C_1 b_{ij} + \varepsilon C_1^n \left(b_{ij}^2 - \frac{1}{3}b_{kk}^2 \delta_{ij}\right) \tag{54}$$

The coefficients C_1 and C_1^n can be functions of the invariants $II_b = (-1/2)b_{kk}^2$, $III_b = (1/3)b_{kk}^3$. Speziale *et al*. (1991) invoked this form with the coefficients

$$C_1 = 1.7 + \frac{0.9\mathcal{P}}{\varepsilon} \quad \text{and} \quad C_1^n = 1.05$$

C_1 was made a function of production over dissipation to incorporate data measured in shear flows.

While there are grounds for including the C_1^n term, as a practical matter nonlinearity can adversely affect numerical convergence when SMC models are used in complex geometries. For instance, the SSG model (Speziale *et al*., 1991) suffers from stiffness unless C_1^n is set to zero; doing so has a negligible effect on predictions in wall bounded flow.

4.2 Models for the rapid part

The rapid part of the $\wp_{ij}$ model is defined as the portion of the model that explicitly involves the tensor components $\partial_i U_j$. A good deal of research on SMC has focused on the rapid pressure-strain model for homogeneous turbulence. In general, the rapid contribution to (52) is represented as

$$\wp_{ij}^{\text{rapid}} = \varepsilon \mathcal{F}_{ij}^{\text{rapid}} = M_{ijkl}\partial_l U_k \tag{55}$$

The various closures amount to different prescriptions of the tensor $\boldsymbol{M}$. Constraints on $\boldsymbol{M}$ can be derived, but there is still considerable freedom in how it is selected. The most common models assume $\boldsymbol{M}$ to be a function of the anisotropy tensor $\boldsymbol{b}$. One way of devising a model is to expand in powers of anisotropy, treating coefficients as empirical constants; an elaboration is to treat the coefficients as functions of the invariants of $\boldsymbol{b}$ – possibly expanding them as well, to be systematic.

When the coefficients are constants and the expansion stops at the linear term in $\boldsymbol{b}$, the general linear model (GLM) is obtained:

$$\begin{aligned}\wp_{ij}^{\text{rapid}} &= \frac{2}{5}k(\partial_j U_i + \partial_i U_j) \\ &\quad + kC_2\left(b_{ik}\partial_k U_j + b_{jk}\partial_k U_i - \frac{2}{3}\delta_{ij}b_{kl}\partial_k U_l\right) \\ &\quad + kC_3\left(b_{ik}\partial_j U_k + b_{jk}\partial_i U_k - \frac{2}{3}\delta_{ij}b_{kl}\partial_k U_l\right)\end{aligned} \tag{56}$$

Special cases of (56) are the LRR (Launder *et al*., 1975) and the isotropization of production (IP), (Noat *et al*., 1973) models.

The formula (56) can be rearranged into other forms that appear in the literature. In terms of the production tensor it becomes

$$\begin{aligned}\wp_{ij}^{\text{rapid}} &= \left[\frac{4}{5} - \frac{4}{3}(C_2 + C_3)\right]kS_{ij} - C_2\left(\mathcal{P}_{ij} - \frac{2}{3}\delta_{ij}\mathcal{P}\right) \\ &\quad - C_3\left(D_{ij} - \frac{2}{3}\delta_{ij}\mathcal{P}\right)\end{aligned} \tag{57}$$

after defining

$$D_{ij} = -\overline{u_i u_k}\partial_j U_k - \overline{u_j u_k}\partial_i U_k$$

The form (57) was introduced by Launder *et al*. (1975). They derived the coefficients

$$C_2 = \frac{c+8}{11} \quad \text{and} \quad C_3 = \frac{8c-2}{11}$$

from certain constraints and selected the empirical constant $c = 0.4$. The IP model uses

$$C_2 = \frac{3}{5} \quad \text{and} \quad C_3 = 0$$

Speziale *et al*. (1991) found that data on shear flow anisotropy were fit by $C_2 = 0.4125$ and $C_3 = 0.2125$ (the seemingly large number of decimal places is due to transforming from their variables to the present). They also added the term

$$-C_s^*\sqrt{\frac{1}{2}b_{ij}b_{ji}}\,kS_{ij} \tag{58}$$

The relative importance of the rapid and slow redistribution models depends somewhat on flow conditions. The split between them for the IP and SSG models is shown in Figure 4 for plane channel flow. The specifics vary with the model, but both rapid and slow components make a significant contribution throughout the flow. One should be warned that the predictions of these models are not correct in the region $y_+ \lesssim 80$. The behavior of D_{ij} near the wall produces quite anomalous predictions by the SSG redistribution model. Methods for correcting the near-wall behavior of quasi-homogeneous models are discussed below.

Closure of equation (50) is effected by replacing $\wp_{ij}$ by the sum of a rapid and a slow model. Physical processes are captured largely through the production tensor, which is exact. The redistribution formulae partially counteract production. For instance, in parallel shear flow, turbulent energy is produced in the streamwise component of intensity and fed to the other components by the redistribution model.

Effects of imposed rotation illustrate the role of the production tensor. In parallel shear flow, $U_1(x_2)$, rotating about the x_3-axis, P_{ij} becomes

$$[P_{ij}] = \begin{pmatrix} 2\overline{u_1u_2}(2\Omega - \partial_2 U_1) & -\overline{u_2^2}\partial_2 U_1 & 0 \\ & +2\Omega(\overline{u_2^2} - \overline{u_1^2}) & \\ -\overline{u_2^2}\partial_2 U_1 + 2\Omega(\overline{u_2^2} - \overline{u_1^2}) & -4\Omega\overline{u_1u_2} & 0 \\ 0 & 0 & 0 \end{pmatrix} \tag{59}$$

Consider a positive imposed angular velocity, $\Omega > 0$. Usually $\overline{u_1u_2}$ is negative if $\partial_2 U_1 > 0$. According to (59) $P_{22} > 0$ in this case, while $P_{22} < 0$ for negative frame rotation. This accounts for the stabilizing or destabilizing

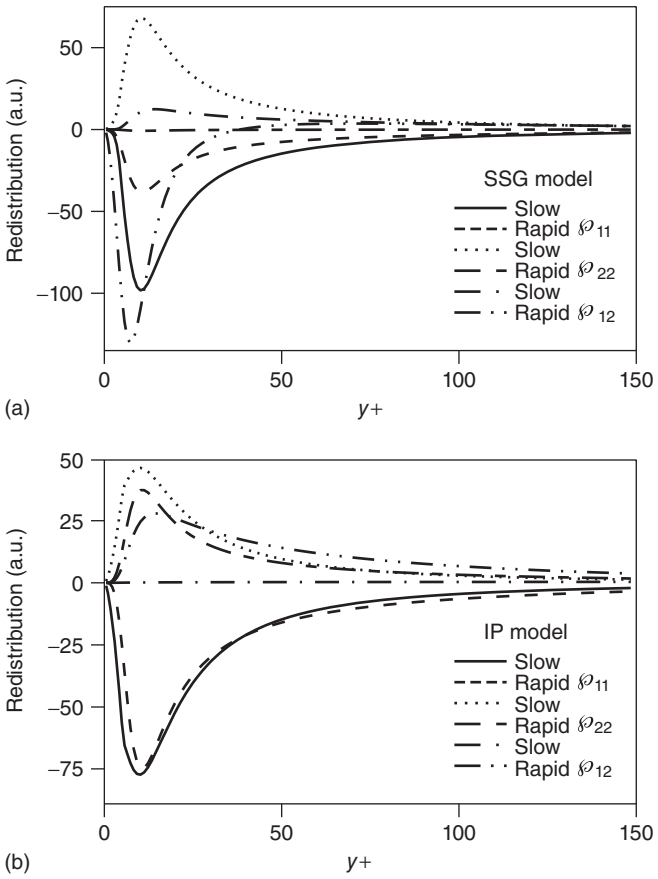

Figure 4. Contributions of the rapid and slow redistribution model in plane channel flow for the SSG and IP models.

tendencies of rotation, or swirl. When the rotation has the opposite sign to the shear, it tends to suppress turbulent energy.

The role of the redistribution tensor usually is to compensate unequal production rates. In the case of (59) it will generate the $\overline{u_3^2}$ component of intensity, which is not produced directly. Symmetry prevents $\overline{u_1 u_3}$ from being generated in this case.

Expression (59) illustrates why SMC can be numerically intransigent: the individual stress components are coupled through the production and redistribution tensors; $\overline{u_1 u_2}$ appears in the $\overline{u_1^2}$ and $\overline{u_2^2}$ equations, $\overline{u_1^2}$ and $\overline{u_2^2}$ appear in the $\overline{u_1 u_2}$-equation, and so on. Computational schemes often treat production explicitly and destruction implicitly. This requires special treatment of source terms, and, in the present case, simultaneous solution of the various components. Usually the latter is not done; hence, failing to couple the components numerically can be a source of computational stiffness.

4.3 Equilibrium approximation

The concept of moving equilibrium was introduced by Rodi (1976). It assumes that the anisotropy tensor (51) asymptotes at large time to a constant value – albeit $\overline{u_i u_j}$ and k remain time dependent. Then, by substituting equation (50) into

$$\partial_t b_{ij} = \frac{\partial_t \overline{u_i u_j}}{k} - \frac{\overline{u_i u_j}\partial_t k}{k^2} = 0 \tag{60}$$

Thereby, an implicit formula for the Reynolds stress as a function of the mean velocity gradient is obtained:

$$\mathcal{P}_{ij} - \frac{2}{3}\delta_{ij}P + \wp_{ij} + (P-\varepsilon)b_{ij} = 0 \tag{61}$$

It is assumed that transport equations will be solved for k and ε.

A model for $\wp_{ij}$ is needed to make (61) concrete. For instance, with the GLM (56) and Rotta (53) models, it becomes

$$\begin{aligned} 0 = {} & (1-C_1)b_{ij}\frac{\varepsilon}{k} - \frac{8}{15}S_{ij} \\ & + (C_2 + C_3 - 1)\left(b_{ik}S_{kj} + b_{jk}S_{ki} - \frac{2}{3}\delta_{ij}b_{kl}S_{lk}\right) \\ & + (C_2 - C_3 - 1)(b_{ik}\Omega_{kj} + b_{jk}\Omega_{ki}) \end{aligned} \tag{62}$$

This can be solved for b_{ij} to obtain the Reynolds stress required by the RANS equations (6).

A closed form solution exists for equation (62), or for fairly general quasi-linear models, such as SSG. The three-dimensional solution is quite unmanageable (Gatski and Speziale, 1993); however, the two-dimensional solution is a nonlinear constitutive model (Section 3.7) of the form (49) with

$$\begin{aligned} C_{\tau_1} &= \frac{(-8/15)\ g}{[1-(2/3)]g^2|S|^2 + 2g^2|\boldsymbol{W}|^2} \\ C_{\tau_2} &= gC_{\tau_1}(1 - C_2 + C_3) \\ C_{\tau_3} &= -2gC_{\tau_1}(1 - C_2 - C_3) \end{aligned} \tag{63}$$

where

$$\begin{aligned} g &= \frac{1}{C_1 - 1 + P/\varepsilon} \\ |\mathcal{S}| &= |\boldsymbol{S}|(1 - C_2 - C_3)\frac{k}{\varepsilon} \\ |\boldsymbol{W}| &= |\boldsymbol{\Omega}|(1 - C_2 + C_3)\frac{k}{\varepsilon} \end{aligned}$$

In practice, the two-dimensional constitutive model (49) with these coefficients is used in fully three-dimensional flow. The

complete equilibrium solution requires that (49) be used to compute P, which becomes a cubic equation for P in the case of (63).

Speziale and Mac Giolla Mhuiris (1989) showed that two solution branches exist in rotating flow. External forces, such as those caused by rotation, can cause one solution branch to disappear at a parameter value. This is referred to as a *bifurcation*, although the use of this term is a bit unconventional. Mathematically the bifurcation explains how SMC models respond to external forces; conceptually, it describes a transition from growing turbulence to decaying turbulence as a stabilizing effect is increased. However, the complete equilibrium solution is not used for predictive purposes; either the nonlinear stress-velocity gradient relation (49), or the algebraic system (62) is invoked as a constitutive model.

Some of the pros and cons of nonlinear constitutive models are discussed in Apsley and Leschziner (1999). The dominant effects arise through the dependence of C_{τ_1} on $\boldsymbol{S}$ and $\boldsymbol{\Omega}$; in other words, they can be represented by a variable C_μ in (12). The latter is the nature of (36) or (43). Other C_μ formulas, often motivated by equilibrium analyses such as that leading to (63), also have been proposed; Mellor and Yamada (1982) do so to obtain effects of density stratification.

4.4 Turbulent transport

There are two critical effects of nonhomogeneity on the mathematical modeling: the turbulent transport terms in the Reynolds stress budget (7) do not vanish and the redistribution models discussed above must be modified for effects of boundaries. Transport terms will be discussed first, and then the more difficult topic of wall effects on the redistribution model is covered.

The Reynolds stress budget (7) contains both turbulent and molecular transport on its right side. For constant density the relevant terms are

$$-\partial_k\left(\overline{u_k u_i u_j} - \frac{2}{3}\frac{\overline{u_k p}}{\rho\delta_{ij}}\right) + \nu\nabla^2\overline{u_i u_j}$$

The second term, molecular transport, is closed and needs no modeling. Oftentimes modeling turbulent transport is characterized as representing $\overline{u_k u_i u_j}$ as a tensor function of $\overline{u_i u_j}$. This philosophy leads to rather complex formulas because the symmetry in i,j,k should be respected. However, the term being modeled is only symmetric in i,j. The three-fold symmetry is not apparent in the RST equation. Hence, there is little motive to constrain the model to satisfy the hidden symmetry – especially when it causes a great deal of added complexity. The inviolable constraints are that the model must preserve the conservation form and be symmetric in i and j.

The notion that the third velocity moment represents random convection by turbulence is invoked. The Markovian assumption, that this can be modeled by gradient diffusion, is made in most engineering models. The most common closure is the Daly and Harlow (1970) formula,

$$-\partial_k\left(\overline{u_k u_i u_j} - \frac{2}{3}\frac{\overline{u_k \partial_k p}}{\rho\delta_{ij}}\right) = \partial_k(C_s T\ \overline{u_k u_l}\partial_l\overline{u_i u_j}) \qquad (64)$$

Here, the eddy viscosity tensor is $C_s\overline{u_k u_l}T \equiv \nu_{T_{kl}}$. A typical value of the empirical constant is $C_s = 0.22$ (Launder, 1989). Near to a wall the dominant component of the gradient is in the wall-normal direction, y. Then (64) is approximately $\partial_y(C_s T\overline{v^2}\partial_y\overline{u_i u_j})$. The dominant eddy viscosity is $\nu_T = C_s T\ \overline{v^2}$. One influence of a wall is to suppress $\overline{v^2}$ relative to the other intensities. With the caveat that the model must be able to predict $\overline{v^2}$ correctly, (64) proves to be more accurate than a simpler model, in which the eddy viscosity scales on the turbulent energy, $\nu_{T_{kl}} = \delta_{kl}C_s Tk$.

The closed RST equation with (64) is

$$\partial_t\overline{u_i u_j} + U_k\partial_k\overline{u_i u_j} = \wp_{ij} - \frac{2}{3}\delta_{ij}\varepsilon + \partial_k(C_s T\ \overline{u_k u_l}\partial_l\overline{u_i u_j}) - \overline{u_j u}_k\partial_k U_i - \overline{u_i u}_k\partial_k U_j + \nu\nabla^2\overline{u_i u_j} \qquad (65)$$

The algebraic formulas in Sections 4.1 and 4.2 can be substituted for $\wp_{ij} = \wp_{ij}^{\text{rapid}} + \wp_{ij}^{\text{slow}}$. This closure can be used to predict free shear flows; but near to walls the algebraic formulas for $\wp_{ij}$ can be rather erroneous.

To skirt the problem, wall function boundary conditions can be applied in the log-layer; in lieu of a suitable model, practical computations often resort to this. The approach is quite similar to the method discussed in connection with the $k-\varepsilon$ model. The wall function consists of adding $\overline{u_i u_j}$to equation (34) by prescribing ratios $\overline{u_i u_j}/k$. In 2-D a suitable set of experimental values is

$$\left\{\frac{\overline{u_i u_j}}{k}\right\} = \begin{pmatrix} 1.06 & -0.32 & 0 \\ -0.32 & 0.42 & 0 \\ 0 & 0 & 0.52 \end{pmatrix} \qquad (66)$$

In 3-D, x_1 is the flow direction and x_2 is normal to the wall. Wall function boundary conditions for $\overline{u_i u_j}$ are harder to justify than the logarithmic specification for U. For instance, the data of DeGraaff and Eaton (2000) show that $\overline{u_i u_j}/k$ is dependent on Reynolds number.

4.5 Near-wall modeling

In an equilibrium boundary layer, the near-wall region refers to the zone from the log-layer to the wall. It includes the viscous dominated region next to the surface and the strongly inhomogeneous region above it. Thus, it is a region in which nonhomogeneity and viscosity play dominant roles. The near-wall region is one of "high impedance" to turbulent transport, in the sense that the wall suppresses the normal component of turbulence. This means that the layer adjacent to the wall controls skin friction and heat transfer disproportionately, making it critical to engineering applications. It is also of great interest to turbulence theory because it is the region of high shear and large rates of turbulence production.

The primary mathematical issues in near-wall modeling are boundary conditions and nonlocal wall effects on redistribution. The issue of nonlocal influences of the wall presents rather a challenge to an analytical model. These wall influences can have pronounced effects. Various methods have been developed to represent nonlocal wall influences. The two discussed in Sections 4.5.2 and 4.5.3 are wall echo and elliptic relaxation.

4.5.1 No-slip

It might seem that the boundary condition at a no-slip wall for the Reynolds stress tensor is simply $\overline{u_i u_j} = 0$. While that is correct, the power of y with which the zero value is approached is often of importance. Models should be designed such that their near-wall asymptotic behavior is reasonable. We will examine the consequences of the no-slip boundary condition on the asymptotic behavior of turbulence statistics near a wall, determining the power of y with which various quantities vary as $y \to 0$.

Let the no-slip wall be the plane $y = 0$. The no-slip condition is that all components of velocity vanish: $\boldsymbol{u} = 0$. Even if the wall is moving, all components of the turbulent velocity vanish, provided the wall motion is not random. If the velocity is a smooth function of y, it can be expanded in a Taylor series,

$$u_i = a_i + b_i y + c_i y^2 \ \ldots$$

where a_i, b_i, and c_i are functions of x and z. The no-slip condition requires that $a_i = 0$. Thus the tangential components satisfy $u = O(y)$, $w = O(y)$ as $y \to 0$. However, the continuity equation, $\partial_y v = -\partial_x u - \partial_z w$ shows that $b_2 = 0$ and thus $v = O(y^2)$. From these limits of the fluctuating velocity, the Reynolds stresses are found to behave like

$$\begin{aligned} &\overline{u^2} = O(y^2); \quad \overline{v^2} = O(y^4); \quad \overline{w^2} = O(y^2) \\ &\overline{uv} = O(y^3); \quad \overline{uw} = O(y^2); \quad \overline{vw} = O(y^3) \end{aligned} \tag{67}$$

as $y \to 0$. The solution to a Reynolds stress model should in principle be consistent with these. However, in practice, it may be sufficient to ensure that $-\overline{uv}$ and $\overline{v^2}$ are small compared to $\overline{u^2}$ when $y_+ \ll 1$. This implements the suppression of normal transport in the immediate vicinity of the wall. The formality $y_+ \ll 1$ can be taken with a grain of salt; the powers (67) are satisfied by experimental data when $y_+ \lesssim 5$.

The limiting behavior of the dissipation rate tensor, $\varepsilon_{ij} = 2\nu(\overline{\partial_i u_j \partial_i u_k})$, is found to be

$$\begin{aligned} &\varepsilon_{11} = O(1); \quad \varepsilon_{22} = O(y^2); \quad \varepsilon_{33} = O(1) \\ &\varepsilon_{12} = O(y); \quad \varepsilon_{13} = O(1); \quad \varepsilon_{23} = O(y) \end{aligned}$$

These are derived by considerations such as $\varepsilon_{12} \to 2\nu(\overline{\partial_y u \partial_y v}) = O(y)$, using the near-wall behavior of the fluctuation velocity cited above. Note that $\varepsilon_{ij} = O(\overline{u_i u_j}/k)$ as $y \to 0$. This proves to be a useful observation about near-wall scaling.

A consideration of the various contributions to the Reynolds stress budget (7) shows that the dominant balance near a surface is between dissipation, molecular diffusion, and the pressure term. The budget reduces simply to

$$\nu \partial_y^2 \overline{u_i u_j} = \varepsilon_{ij}$$

if i and j are not 2, and to

$$\nu \partial_y^2 \overline{u_i u_j} = \overline{u_i \partial_j p} + \overline{u_j \partial_i p} + \varepsilon_{ij}$$

if i or j equals 2. The first recovers the limit

$$\varepsilon_{ij} \to \frac{2\nu \overline{u_i u_j}}{y^2} \approx \frac{\overline{u_i u_j}\varepsilon}{k}$$

if $i, j \neq 2$; the second shows that ε_{ij} is of the same order in y as $\overline{u_i u_j}\varepsilon/k$, although not exactly equal to it.

4.5.2 Wall echo

The elliptic nature of wall effects was recognized early in the literature on turbulence modeling and has continued to influence thoughts about how to incorporate nonlocal influences of boundaries (Launder *et al.*, 1975; Durbin, 1993; Manceau *et al.*, 2001).

In the literature on closure modeling the nonlocal effect is often referred to as "pressure reflection" or "pressure echo" because it originates with the surface boundary condition imposed on the Poisson equation for the perturbation pressure. The boundary condition influences the pressure interior to the fluid, which can be described as a nonlocal, kinematic effect.

The velocity–pressure gradient correlation that appears in the redistribution term must be corrected for the wall influence. In the wall echo approach, it is taken to be an additive correction

$$\wp_{ij} = \wp^h_{ij} + \wp^w_{ij} \tag{68}$$

The $\wp^h_{ij}$ term represents one of the models developed above, such as the GLM (57) plus the Rotta return to isotropy (53).

The additive wall correction $\wp^w_{ij}$ is often referred to as *the wall echo contribution*. It is modeled as a function of the unit wall normal $\hat{n}$ and of the shortest distance to the wall, d. A simple example is the formula

$$\begin{aligned}\wp^w_{ij} = &-C^w_1 \frac{\varepsilon}{k}\left[\overline{u_i u_m}\hat{n}_m\hat{n}_j + \overline{u_j u_m}\hat{n}_m\hat{n}_i - \frac{2}{3}\overline{u_m u_l}\hat{n}_m\hat{n}_l\delta_{ij}\right]\frac{L}{d} \\ &- C^w_2\left[\wp^{\text{rapid}}_{im}\hat{n}_m\hat{n}_j + \wp^{\text{rapid}}_{jm}\hat{n}_m\hat{n}_i - \frac{2}{3}\wp^{\text{rapid}}_{ml}\hat{n}_m\hat{n}_l\delta_{ij}\right]\frac{L}{d}\end{aligned} \tag{69}$$

proposed by Gibson and Launder (1978). Here $L = k^{3/2}/\varepsilon$ and the $\hat{n}_i$ are components of the unit wall normal vector. The factor of L/d causes this correction to vanish far from the surface. The idea is that wall effects decay at a distance on the order of the correlation scale of the turbulent eddies. Gibson and Launder (1978) used (69) in conjunction with the IP model for $\wp^{\text{rapid}}$. The model constants $C^w_1 = 0.3$ and $C^w_2 = 0.18$ were suggested.

If the wall normal is the x_2-direction then the rapid contribution to the 22-component of (69) is

$$\wp^w_{22} = -\frac{4}{3}C^w_2\wp^{\text{rapid}}_{22}\frac{L}{x_2}$$

for the wall normal intensity. In shear flow parallel to the wall, energy is redistributed from $\overline{u^2}$ into $\overline{v^2}$ so $\wp^{\text{rapid}}_{22} > 0$. With $\wp^{\text{rapid}}_{22} > 0$ the wall correction is negative. This is consistent with the idea that blocking suppresses the wall normal component of intensity.

However, in a flow toward the wall the velocity has a component $V(y)$. On the stagnation streamline the mean rate of strain $\partial_y V$ will produce $\overline{v^2}$ and energy will be redistributed out of this component: $\wp^{\text{rapid}}_{22} < 0$, so the wall correction, stated above, is positive. It therefore has the erroneous effect of enhancing the normal component of intensity. Craft *et al*. (1993) proposed a more complex wall echo function to correct this fault.

The formula (69) illustrates that wall corrections are tensoral operators that act on the Reynolds stress tensor. The $\hat{n}_i$ dependence of these operators has to be adjusted to properly damp each component of $\overline{u_i u_j}$. The formula for the correction function, $\wp^w_{ij}$, has to be readjusted in a suitable manner for each homogeneous redistribution model to which it is applied. For instance, the relative magnitudes of the rapid and slow contributions to $\wp_{ij}$ differ between the IP and SSG models. This demands that wall echo be adapted differently in each instance. Lai and So (1990) present a wall echo function for the SSG model.

4.5.3 Elliptic relaxation and elliptic blending

Elliptic relaxation (Durbin, 1993) is a rather different approach to wall effects. It is incorporated by solving an elliptic equation. Contact with homogeneous redistribution models, such as those described in Section 4, is made via the source term in the elliptic equation. The particular equation is of the modified Helmoltz form:

$$L^2\nabla^2 f_{ij} - f_{ij} = -\frac{\wp^h_{ij} + \varepsilon b_{ij}}{k} \equiv -\frac{\wp^{qh}_{ij}}{k} \tag{70}$$

On the right side, the superscript qh acknowledges that this is the quasi-homogeneous model. To use this method, the RST equation is rewritten as

$$D_l\overline{u_i u_j} + \varepsilon\frac{\overline{u_i u_j}}{k} = \mathcal{P}_{ij} + \wp_{ij} + \partial_k[\nu_{T_{kl}}\partial_l\overline{u_i u_j}] + \nu\nabla^2\overline{u_i u_j} \tag{71}$$

f_{ij} is an intermediate variable, related to the redistribution tensor by $\wp_{ij} = kf_{ij}$. The solution to (70) provides the nonhomogeneous model. The turbulent kinetic energy, k, is used as a factor in order to enforce the correct behavior, $\wp_{ij} \to 0$, at a no-slip boundary (Section 4.5.1).

The anisotropic influence of the wall on Reynolds stresses interior to the fluid arises by imposing suitable boundary conditions on the components of the $\overline{u_i u_j} - f_{ij}$ system. Boundary conditions are described in Section 5.1. The wall normal now enters only into the wall boundary condition.

The length scale in (70) is prescribed by analogy to (22) as

$$L = \max\left[c_L\frac{k^{3/2}}{\varepsilon}, c_\eta\left(\frac{\nu^3}{\varepsilon}\right)^{1/4}\right] \tag{72}$$

In fully turbulent flow it has been found that Kolmogoroff scaling collapses near-wall data quite effectively (Laurence, 2002; Manceau *et al*., 2001). Hence the Kolmogoroff scale is used for the lower bound in (72). The important feature is that L and T do not vanish at no-slip surfaces. If they vanished then the equations would become singular.

The elliptic relaxation procedure (70) accepts a homogeneous redistribution model on its right side and operates on it with a Helmholtz type of Green's function, imposing suitable wall conditions. The net result can be a substantial

alteration of the near-wall behavior from that of the original redistribution model. The $v^2 - f$ and $\zeta - f$ models (Hanjalic *et al*., 2005) are scalar, eddy viscosity application of elliptic relaxation.

Elliptic blending invokes the f-equation

$$L^2 \nabla^2 f - f = -1 \tag{73}$$

Manceau (2015) uses f^2 to interpolate between the near wall redistribution model and the main flow. The boundary conditions are $f = 0$ at the wall and $f \to 1$ at infinity. For instance, the pressure strain is written as

$$\wp_{ij} = f^2 \wp_{ij}^h + (1 - f^2)\wp_{ij}^w$$

This is a source term in RST equations. A unit vector $\hat{n} = \nabla f / |\nabla f|$ replaces the wall normal, which appears in earlier formulations of $\wp_{ij}^w$.

5 REYNOLDS-AVERAGED COMPUTATION

Closure models are ultimately meant to be used in CFD codes for the purpose of predicting mean flow fields, and possibly the Reynolds stress components. The only information that they can provide is these low order statistics. RANS computations do not simulate random eddying, although quite complex mean flows are routinely calculated.

Standard discretization methods (see **Finite Difference Methods**, **Finite Element Methods**) can be applied to turbulent transport equations, such as those for k, ε, or $\overline{u_i u_j}$. The relevant chapters **Finite Difference Methods**, **Finite Element Methods** should be consulted on matters of numerical analysis. The following section is a brief mention of a few special topics that bear specifically on solving the closure models.

5.1 Numerical issues

Most practical engineering computations are done with some variety of eddy viscosity formulation (Section 3). Second moment closures (Section 4) promise greater fidelity to turbulence physics (Hanjalic, 1994); however, the computational difficulties they present are manifold. The absence of numerically stabilizing, eddy viscous terms, in the mean flow equations, the strong coupling between Reynolds stress components via production and redistribution, the increased number of equations, and other computationally adverse properties lead to slow, tenuous convergence. Special methods that overcome this have been explored; the work of Leschziner and Lien (2002) provides many suggestions. By contrast, eddy viscosities, as a rule, assist convergence. The tendency for the flow equations to develop chaotic solutions is overcome by eddy viscous dissipation.

It is common practice to decouple the turbulence model solver from the mean flow solver. The only communication from the model might be an eddy viscosity that is passed to the mean flow. The mean flow solver would then compute the Navier–Stokes equations with variable viscosity. Most applied CFD codes incorporate a selection of more than one eddy viscosity scheme; isolating the model solution from the mean flow solution simplifies implementation of the various models.

It is not just the plethora of models that motivates a segregated solution. Sometimes different algorithms are used to solve each portion. As a rule, turbulence models are solved more readily with implicit numerical schemes, while explicit schemes are sometimes preferred for the mean flow (Turner and Jenions, 1993). A case in point is provided by the Spalart–Allmaras model: explicit methods are popular for compressible aerodynamic flows; the S–A eddy viscosity transport model (Section 3.6) is also popular for aerodynamics; unfortunately, there has been little success solving S–A with explicit schemes. On the other hand, the S–A equations are readily integrated with alternating direction implicit (ADI) or other implicit methods.

It has been argued that first order, upwind discretization of the convective derivative is acceptable for the turbulence variables, even though such low accuracy usually is not acceptable for the mean flow. A rationale is that the turbulence equations are dominated by source and sink terms, so inaccuracies in the convection term are quantitatively small. In most cases, this line of reasoning has been verified. However, where production is small, or changes are rapid, local inaccuracies exist. A common strategy is to first compute a preliminary solution with first-order convection, then to reconverge it with higher order accuracy. In the same vein, an eddy viscosity solution is sometimes used to initiate a second moment computation.

A general rule of thumb is to make dissipation implicit and production explicit. More exactly, treat these source terms so as to improve diagonal dominance. This rule of thumb generalizes to the evolution equation for any variable ϕ, where ϕ would be k in the k-equation, or $\overline{u_i u_j}$ in a Reynolds stress equation. In order to distinguish the implicit and explicit parts, the source term is arranged into the form $A - B\phi$ where $A, B \geq 0$; that is, the evolution equation is put into the form

$$D_t \phi = A - B\phi + \cdots$$

where A and B can be functions of the dependent variables. The rule of thumb for treating dissipation and production is implemented by updating the source term as $A^n - B^n \phi^{n+1}$.

However, the splitting between the explicit contribution A and the implicit contribution $B\phi$ is not unique. As an example of the leeway, consider the right side of the k-equation: $\mathcal{P} - \varepsilon$ might be rewritten as $\mathcal{P} - (\varepsilon/k)k$ for which $A = \mathcal{P}$ and $B = \varepsilon/k$. The update is then

$$\mathcal{P}^n - \left|\frac{\varepsilon^n}{k^n}\right| k^{n+1}$$

the absolute value ensures that $B \geq 0$. In this same vein, Spalart and Allmaras (1992) recommend treating the sum of production and dissipation implicitly or explicitly depending on the sign of its Jacobian. After rewriting $P_\nu - \varepsilon_\nu$ in (44) exactly in the form $(JP - J\varepsilon)\tilde{\nu}$, they then construct the source as

$$(P_\nu - \varepsilon_\nu)^n - \text{pos}[(J\varepsilon - JP)^n]\Delta\tilde{\nu} - \text{pos}[\partial_\nu(J\varepsilon - JP)\nu^n]\Delta\tilde{\nu}$$

where $\text{pos}(x) = (x + |x|)/2$ and $\Delta\tilde{\nu} = \tilde{\nu}^{n+1} - \tilde{\nu}^n$.

Leschziner and Lien (2002) discuss the treatment of source terms in SMCs. Numerical stiffness is often encountered when solving transport models for $\overline{u_i u_j}$. The root cause is the functional coupling between the Reynolds stress components introduced by the production and redistribution tensors. For example, the evolution equation for $\overline{uv}$ contains $\overline{v^2}\partial_y U$ in the production term, and the equation for $\overline{v^2}$ contains $\overline{uv}\partial_y U$ in the redistribution term. When $\overline{uv}$ and $\overline{v^2}$ are solved separately – often called a segregated solution – justice is not done to this intimate coupling. On occasion it has been proposed to solve the full set of components simultaneously, as a coupled system (Laurence, 2002). However, no general scheme has been offered for robustly solving RST equations.

The Reynolds stress appears as a body force if it is treated explicitly in the mean flow equation (6). But the Reynolds stress is inherently a diffusive term that should provide numerical stability. To recover the diffusive property, eddy diffusion can be subtracted from both sides of the mean flow equation, treating it implicitly on one side and explicitly on the other, as in

$$\begin{aligned}\partial_t U_i + U_j\partial_j U_i - \partial_j[\nu_T(\partial_j U_i + \partial_i U_j)]^{(n+1)} &= -\frac{1}{\rho}\partial_i P \\ + \nu\nabla^2 U_i - \partial_j\overline{u_j u_i}^{(n)} - \partial_j[\nu_T(\partial_j U_i + \partial_i U_j)]^{(n)} &\end{aligned} \tag{74}$$

The procedure (74) will be the most effective if

$$\overline{u_i u_j} - \frac{2}{3}k\delta_{ij} + \nu_T(\partial_j U_i + \partial_i U_j)$$

is made small. In practice, simply using the $k - \varepsilon$ formula (11) for ν_T in equation (74) adds greatly to the ease of convergence.

Boundary conditions can be problematic when the $k - \varepsilon$ model is integrated to a no-slip wall.

$$\varepsilon(0) = 2\nu \lim_{y\to 0}\left[\frac{k(y)}{y^2}\right] \tag{75}$$

is usually invoked, per (20). A ratio evaluated at the first computational point from the wall is substituted for the limit on the left side. The factor of y^{-2} can cause stiffness if this condition is not implemented implicitly. (If the k and ε equations are coupled, (19) can be used to avoid the y^{-2}.)

The singular boundary condition to the $k - \omega$ model (Section 3.5) is

$$\omega(0) = \lim_{y\to 0}\left[\frac{6\nu}{C_{\omega 2}y^2}\right] \tag{76}$$

Wilcox (1998) suggests specifying this as the solution for the first few grid points; Menter (1992) recommends using $\omega = 10[6\nu/(C_{\omega 2}y_1^2)]$ as the boundary value. The factor of 10 is arbitrary, but Menter states that the results are not sensitive to the precise value.

Modifications to turbulence models that are made for numerical reasons can result in inconsistent predictions. Rumsey (2009) has created a website with solutions for verifying consistent implementation of several popular models.

5.2 The assessment of models

A good deal of literature deals with assessment of the predictive accuracy of models. These endeavors tend to be anecdotal and rarely are models dismissed unequivocally. Nevertheless, some remarks will be made on the relative merits of different models.

A large number of variants on basic formulations described herein can be found. To an extent, that is a reflection of the degrees of freedom introduced by empirical content. At times the number of variations on a theme can be overwhelming. But that should not distract from the fact that the number of basic formulations is few: eddy viscosity transport, two-equation, Reynolds stress transport (SMC). The second two categories include another equation to determine a turbulent time scale, via either ω or ε. The equations are of convection–diffusion form, with production and dissipation appearing as source terms, and in the case of SMC, as a redistribution term linking the components (Section 4).

Near-wall modeling can play a disproportionate role because that is a region of reduced turbulent mixing, and hence it can be rate limiting. It adds further degrees of freedom; nevertheless models again can be classified into a few varieties – wall functions, damping functions, two-layers, elliptic relaxation – and the pros and cons assessed for each class.

Factors that tend to distinguish the models are their ability to predict flow separation, surface heat transfer, or the influence of surface curvature and system rotation. Bardina *et al*. (1997) compared two-equation and eddy viscosity transport models, largely on the basis of their ability to predict separation. They favored the SST (equation 36, *ff*.) and S–A (Section 3.6) models over $k-\omega$ and low Reynolds number $k-\varepsilon$. S–A was preferred on numerical grounds and because of its satisfactory predictive accuracy. In this study and others, $k-\varepsilon$ with wall functions was found unreliable for predicting flow separation; its tendency is to predict attached flow beyond the point at which it should separate.

Iacovides and Raisee (1999) have concluded that heat transfer prediction argues for integration to the wall, rather than resorting to wall functions (Section 3.4). Again, low Reynolds number $k-\varepsilon$ (equation (25)) was not recommended. In this study, RST was favored because it responds to curvature in a natural way. It is safe to say that when such effects significantly influence the turbulent intensity, RST formulations are more reliable than scalar formulations. For instance, suppression of turbulent energy in a strongly swirling flow can be captured, as illustrated by Figure 5. In this geometry, the flow enters at the top, as shown in the figure, then swirls round toward the closed lower end. The stabilizing centrifugal acceleration suppresses turbulence in the vicinity of $r = 0$ and permits an upward jet along the axis, as shown by the experimental data and the second moment closure model (Section 4).

Scalar models (Section 3) are insensitive to centrifugal stabilization. In the scalar model case of Figure 5, the fluid stays turbulent near the axis and the flow is downward at the center, with a slow upward flow next to the walls – quite differently from the experiment. It should be mentioned, however, that scalar models can be modified to incorporate rotational stabilization (Durbin, 2011). Such approaches are less reliable than SMC and are used for simplification.

However, when influences such as swirl or streamline curvature have a secondary effect, scalar models can be as good as, or better than, SMC: swirling flow in a pipe expansion can be predicted adequately by a scalar model because centrifugal and pressure gradient effects on the mean flow are captured by the averaged Navier–Stokes equation, and the direct swirl effect on the turbulence is secondary.

A wall echo of the form (69) was invoked by Iacovides and Raisee (1999), but with some additional terms and factors. Because of the latter, evaluations of this type are of limited guidance; those that adhere to widely used forms of the considered models are more suited to advisory tasks. Iacovides and Raisee (1999) concluded that some such form of wall treatment is preferred to wall functions, but that the formulation in equation (69) is not reliable. Elliptic blending

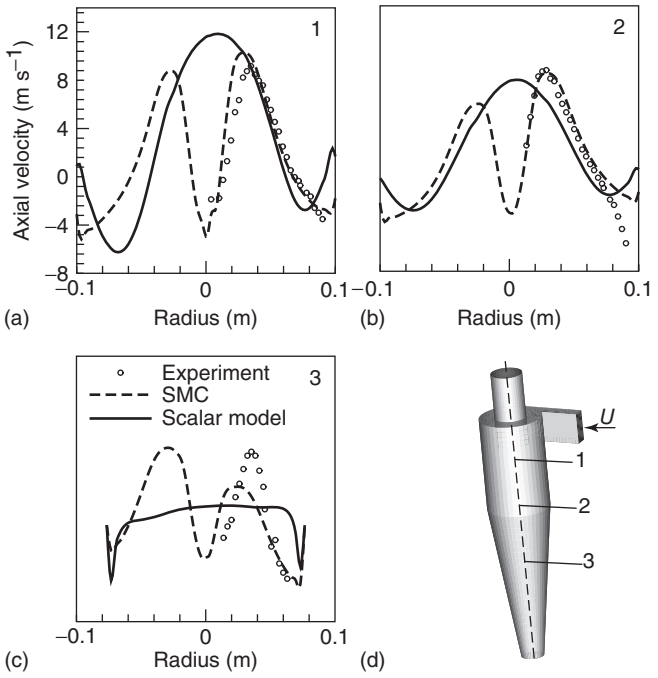

Figure 5. Flow in a cyclone swirler illustrates the failure of scalar models in a flow that is stabilized by swirl. (Reproduced with permission from G. Iaccarino. © G. Iaccarino, 2004.)

provides a more generic, and often more accurate, approach but adds expense; suffice it to say that near-wall treatments for SMC are too insecure to warrant a recommendation on which is most effective. In practice, it is common to use wall functions (equation 66), or a variant of the two-layer approach (Section 3.3).

Ooi *et al*. (2002) found that heat transfer predictions are strongly dependent on the eddy viscosity distribution very near to the surface. In a flat plate boundary layer, ν_T becomes equal to ν when $y_+ \approx 10$. If a model predicts that the eddy viscosity remains higher than molecular viscosity significantly below this, heat transfer will be overpredicted and *vice versa*. In Ooi *et al*. (2002), both the S–A model and the two-layer $k-\varepsilon$ model (Section 3.3) severely underpredicted heat transfer in a ribbed, square duct flow. This could be traced to underprediction of ν_T adjacent to the wall. The v^2-f model was found to be more accurate. The ribs in this geometry cause complex secondary flows and large separation bubbles. One might hope that the principle here is that models using length scales that are prescribed functions of wall distance are less flexible than those based on local variables. S–A and two-layer models are of the former ilk, while v^2-f is of the latter; however, the evidence in favor of the aforementioned principle is not compelling.

Apsley and Leschziner (1999) report on a collaborative assessment of closure schemes. They consider the gamut

from quasilinear eddy viscosity, to nonlinear constitutive equations (equation 49), to full RST. Their study inferred little value from nonlinear constitutive formulations, finding that the linear constitutive relation (12), modified by adding strain-rate dependence to C_μ in (11), constitutes a more effective formulation. In particular the SST model, as an instance of modified C_μ, was a great improvement over the native $k-\omega$ formulation (35). In that case, response to pressure gradients is made more accurate by (in effect) making C_μ depend on the rate of strain. Leading order effects of curvature and system rotation can be incorporated by variable C_μ as well.

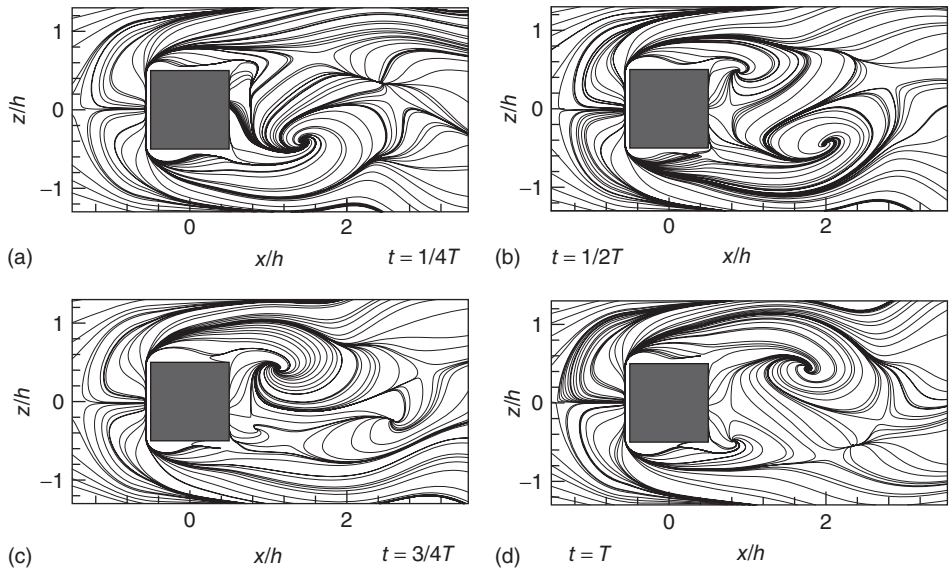

Figure 6. Skin friction lines in periodic flow round a surface mounted cube. (Reproduced with permission from Iaccarino *et al*., 2002. © Elsevier, 2002.)

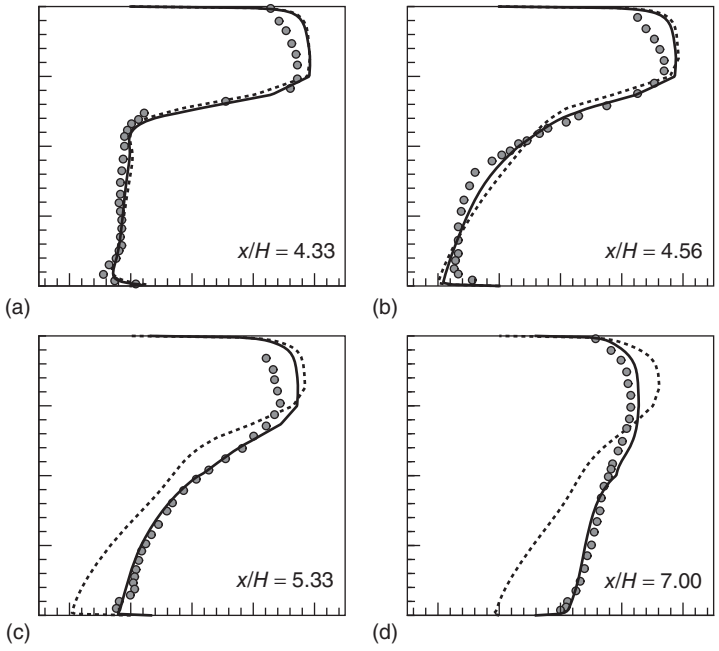

Figure 7. Velocity profiles downstream of the cube, showing the difference between steady (· · · · · · · · ·) and time-averaged unsteady (——) computations. (Reproduced with permission from Iaccarino *et al*., 2002. © Elsevier, 2002.)

Generally, Apsley and Leschziner (1999) found $k-\varepsilon$ formulations to be unsatisfactory. There is an emerging sentiment that, among two-equation formulations, $k-\omega$ variants tend to be more satisfactory than $k-\varepsilon$; but the need for fixes of the large strain anomaly and the free-stream sensitivity, discussed in Section 3.5, should not be overlooked. Also, the singular behavior of ω as a wall is approached can impose stringent grid requirements.

Turbulence models represent averaged effects of random eddying. This is the ensemble average, defined by equation (1). Statistical averaging is not synonymous with time-averaging; Nevertheless, there is frequently a confusion between ensemble and time-averaging. For this reason, it has become usual to refer to *unsteady* RANS when time-dependent flow is computed. A very intriguing application of unsteady RANS (a.k.a. URANS) is to bluff body flows with periodic vortex shedding. In this case the turbulence model represents the broad-band component of the frequency spectrum of the velocity field. The shedding frequency and its harmonics are spikes in the spectrum that are *deterministic* eddies, such as the vonKarman vortex street. These are part of the mean flow and hence must be computed explicitly. Often a steady solution can be obtained by imposing a symmetry on the calculation. However, the steady solution generally underpredicts mixing and overpredicts the length of wakes. Errors associated with steady calculation of unsteady flows are mistakes in the mean flow, and should not be attributed to the turbulence model.

Figure 6 shows skin friction lines in periodic flow round a surface mounted cube (from Iaccarino *et al*., 2002). The flow develops periodic unsteadiness in the immediate lee of the cube. The spiral nodes are a footprint of vortices that arch over the cube. The bands near the top and bottom of each panel are caused by vortices that wrap around the front of the cube.

The comparison in Figure 7 illustrates how a steady computation of this flow is inaccurate, while a time average of an unsteady computation agrees nicely with data. The steady calculation shows a wake extending too far downstream. It omits the component of mixing produced by the unsteady mean flow vortices. Comparison to the unsteady RANS simulation gives an idea of the contribution of mean flow vortices to mixing.

REFERENCES

Apsley DD and Leschziner MA. Advanced turbulence modelling of separated flow in a diffuser. *Flow, Turbul. Combust.* 1999; **63**:81–112.

Baldwin BS and Barth TJ. A one-equation turbulence transport model for high Reynolds number wall-bounded flows. NASA TM-102847, 1990.

Bardina JE, Huang PG and Coakley TJ. Turbulence modeling validation. AIAA Paper 97–2121, 1997.

Barre S, Bonnet J-P, Gatski TB and Sandham ND. Compressible, high speed flow. In *Closure Strategies for Turbulent and Transitional Flows*, Launder BE and Sandham ND (eds). Cambridge University Press: Cambridge, 2002; 522–581.

Chen C-J and Patel VC. Near-wall turbulence models for complex flows including separation. *AIAA J.* 1998; **26**:641–648.

Craft T, Graham L and Launder BE. Impinging jet studies for turbulence model assessment-II: An examination of the performance of four turbulence models. *Int. J. Heat Mass Transfer* 1993; **36**:2685–2697.

Craft T, Iacovides H and Yoon JH. Progress in the use of non-linear two-equation models in the computation of convective heat-transfer in impinging and separated flows. *Flow, Turbul. Combust.* 1999; **63**:59–80.

Daly BJ and Harlow FH. Transport equations of turbulence. *Phys. Fluids* 1970; **13**:2634–2649.

DeGraaff DB and Eaton J. Reynolds number scaling of the flat plate turbulent boundary layer. *J. Fluid Mech.* 2000; **422**:319–386.

Durbin PA. Near-wall turbulence closure modeling without 'damping functions'. *Theor. Comput. Fluid Dyn.* 1991; **3**:1–13.

Durbin PA. A Reynolds stress model for near-wall turbulence. *J. Fluid Mech.* 1993; **249**:465–498.

Durbin PA. Review: adapting scalar turbulence closure models for complex turbulent flows. *J. Fluids Eng.* 2011; **133**:061205-1–8.

Durbin PA and Pettersson Reif BA. *Statistical Theory and Modeling for Turbulent Flow* (2nd edn). John Wiley & Sons, Ltd: Chichester, 2010.

Gatski TB and Speziale CG. On explicit algebraic stress models for complex turbulent flows. *J. Fluid Mech.* 1993; **254**:59–78.

Gibson MM and Launder BE. Ground effects on pressure fluctuations in the atmospheric boundary layer. *J. Fluid Mech.* 1978; **86**:491–511.

Goodbody AM. *Cartesian Tensors*. Ellis Horwood: Chichester, 1982.

Hanjalic K. Advanced turbulence closure models: a view of current status and future prospects. *Int. J. Heat Fluid Flow* 1994; **15**:178–203.

Hanjalic K, Popovac M and Hadziabdic M. A robust near-wall elliptic relaxation eddy-viscosity turbulence model for CFD. *Int. J. Heat Fluid Flow* 2005; **25**:1047–1051.

Iaccarino G, Ooi A, Durbin PA and Behnia M. Reynolds averaged simulation of unsteady separated flow. *Int. J. Heat Fluid Flow* 2002; **24**:147–156.

Iacovides H and Raisee M. Recent progress in the computation of flow and heat transfer in internal cooling passages of turbine blades. *Int. J. Heat Fluid Flow* 1999; **20**:320–328.

Jones WP and Launder BE. The prediction of laminarization with a two-equation model. *Int. J. Heat Mass Transfer* 1972; **15**:301–314.

Kalitzen G, Medic G, Iaccarino G and Durbin PA. Near-wall behavior of RANS turbulence models and implications for wall functions. *J. Comput. Phys.* 2005; **204**:265–291.

Kok J. Resolving the dependence on freestream values for the $k-\omega$ turbulence model. *AIAA J.* 2000; **38**:1292–1295.

Lai YG and So RMC. On near-wall turbulent flow modelling. *AIAA J.* 1990; **34**:2291–2298.

Launder BE. Second-moment closure: present … and future. *Int. J. Heat Fluid Flow* 1989; **10**:282–300.

Launder BE and Kato M. Modelling flow-induced oscillations in turbulent flow around a square cylinder. *ASME FED* 1993; **157**:189–199.

Launder BE and Sharma BL. Application of the energy-dissipation model of turbulence to the calculation of flow near a spinning disk. *Lett. Heat Mass Transfer* 1974; **1**:131–138.

Launder BE and Spalding B. The numerical computation of turbulent flows. *Comput. Methods Appl. Mech. Eng.* 1974; **3**:269–289.

Launder BE, Reece GJ and Rodi W. Progress in the development of a Reynolds stress turbulence closure. *J. Fluid Mech.* 1975; **68**:537–566.

Laurence D. *Applications of RANS Equations to Engineering Problems*, *Von Karman Institute Lecture Series: Introduction to Turbulence Modelling, VKI-LS 1997-03*, Rhode Saint Genese, Belgium: Von Karman Institute for Fluid Dynamics, 2002.

Leschziner MA and Lien FS. Numerical aspects of applying second-moment closure to complex flow. In *Closure Strategies for Turbulent and Transitional Flows*, Launder BE and Sandham ND (eds). Cambridge University Press: Cambridge, 2002; 153–187.

Manceau R. Recent progress in development of the elliptic blending Reynolds-stress model. *Int. J. Heat Fluid Flow* 2015; **51**:195–220.

Manceau R, Wang M and Laurence D. Inhomogeneity and anisotropy effects on the redistribution term in Reynolds-averaged Navier–Stokes modelling. *J. Fluid Mech.* 2001; **438**:307–338.

Mellor GL and Yamada T. Development of a turbulence closure model for geophysical fluid problems. *Rev. Geophys. Space Phys.* 1982; **20**:851–875.

Menter FR. Two-equation eddy-viscosity turbulence models for engineering applications. *AIAA J.* 1992; **32**:1598–1605.

Moser RD, Kim J and Mansour NN. Direct numerical simulation of turbulent channel flow up to $Re_\tau = 590$. *Phys. Fluids* 1999; **11**:943–945.

Noat D, Shavit A and Wolfshtein M. Two-point correlation model and the redistribution of Reynolds stresses. *Phys. Fluids* 1973; **16**:738–743.

Ooi A, Iaccarino G, Durbin PA and Behnia M. Reynolds averaged simulation of flow and heat transfer in ribbed ducts. *Int. J. Heat Fluid Flow* 2002; **23**:750–757.

Parneix S, Durbin PA and Behnia M. Computation of 3-D turbulent boundary layers using the v^2-f model. *Flow, Turbul. Combust.* 1998; **10**:19–46.

Patel VC, Rodi W and Scheurer G. Turbulence modeling for near-wall and low Reynolds number flows: a review. *AIAA J.* 1984; **23**:1308–1319.

Pope SB. A more general effective-viscosity hypothesis. *J. Fluid Mech.* 1975; **72**:331–340.

Pope SB. *Turbulent Flows*. Cambridge University Press: Cambridge, 2000.

Rodi W. A new algebraic relation for calculating the Reynolds stresses. *Z. Angew. Math. Mech.* 1976; **56**:T219–T221.

Rodi W. Experience using two-layer models combining the $k-\varepsilon$ model with a one-equation model near the wall. AIAA Paper 91–0609, 1991.

Rumsey C. Consistency, verification and validation of turbulence models for Reynolds-averaged Native-Stokes applications. *3rd European Conference for Aerospace Sciences* Paper –EUCASS2009-7, 2009.

Spalart PR and Allmaras SR. A one-equation turbulence model for aerodynamic flows. AIAA Paper 92–0439, 1992.

Speziale CG and Mac Giolla Mhuiris N. On the prediction of equilibrium states in homogeneous turbulence. *J. Fluid Mech.* 1989; **209**:591–615.

Speziale CG, Sarkar S and Gatski TB. Modeling the pressure-strain correlation of turbulence: an invariant dynamical systems approach. *J. Fluid Mech.* 1991; **227**:245–272.

Taylor GI. Diffusion by continuous movements. *Proc. London Math. Soc.* 1921; **20**:196–212.

Townsend AA. *The Structure of Turbulent Shear Flow*. Cambridge University Press: Cambridge, 1976.

Turner MG and Jenions IK. An investigation of turbulence modeling in transonic fans including a novel implementation of an implicit $k-\varepsilon$ turbulence model. *ASME J. Turbomach.* 1993; **115**:248–260.

Vieser W, Esch T and Menter FR. Heat transfer predictions using advanced two-equation turbulence models. Technical Memorandum CFX-VAL10/0602, 2002.

White FM. *Viscous Fluid Flow* (2nd edn). McGraw-Hill: New York, 1991.

Wilcox DC. *Turbulence Modeling for CFD* (2nd edn). DCW Industries, Inc.: La Canada CA, 1998.

Wolfshtein M. The velocity and temperature distribution in one-dimensional flow with turbulence augmentation and pressure gradient. *Int. J. Heat Mass Transfer* 1969; **12**:301–318.